DP-MS--82-49

DE83 004913

DP-MS-82-49

Conf-8210112--1

# SURFACE STUDIES OF IRIDIUM-ALLOY GRAIN BOUNDARIES ASSOCIATED WITH WELD CRACKING

by

W. Clanton Mosley

E. I. du Pont de Nemours & Co.
Savannah River Laboratory
Aiken, South Carolina 29808

MASTER

For presentation at the
11th Conference on Surface Studies and 6th SUBWOG-12B
Technical Exchange, Los Alamos, New Mexico
October 5-8, 1982

**NOTICE**

**PORTIONS OF THIS REPORT ARE ILLEGIBLE. It has been reproduced from the best available copy to permit the broadest possible availability.**

This paper was prepared in connection with work done under Contract No. DE-AC09-76SR00001 with the U. S. Department of Energy. 

## DISCLAIMER

# SURFACE STUDIES OF IRIDIUM-ALLOY GRAIN BOUNDARIES ASSOCIATED WITH WELD CRACKING*

by

W. Clanton Mosley

E. I. du Pont de Nemours & Co.
Savannah River Laboratory
Aiken, South Carolina 29808

## ABSTRACT

Plutonium-238 oxide fuel pellets for the General Purpose Heat Source (GPHS) Radioisotopic Thermoelectric Generators to be used on the NASA Galileo Mission to Jupiter and the International Solar Polar Mission are produced and encapsulated in iridium alloy at the Savannah River Plant (SRP). Underbead cracks occasionally occur in the girth weld on the iridium-alloy-clad vent sets in the region where the gas tungsten arc is quenched. Grain-boundary structures and compositions were characterized by scanning electron microscopy/x-ray energy spectroscopy, electron microprobe analysis and scanning Auger microprobe analysis to determine the cause of weld quench area cracking. Results suggest that weld quench area cracking may be caused by gas porosity or liquation in the grain boundaries.

## INTRODUCTION

During encapsulation of plutonium-238 oxide pellets in DOP-26 iridium alloy clad vent sets in the Plutonium Fuel Form (PuFF) Facility at the Savannah River Plant (SRP), intergranular underbead weld cracks occasionally occur in the girth weld on the DOP-26 iridium alloy clad vent sets in the area where the gas tungsten arc is quenched. Scanning electron microscopy/x-ray energy spectroscopy (SEM/XES), electron microprobe analysis (EMPA) and scanning Auger microprobe (SAM) analysis have been used by the Savannah River Laboratory (SRL) to characterize grain boundary structures and compositions in an effort to identify the cause of cracking.

---

* The information contained in this article was developed during the course of work under Contract No. DE-AC09-76SR00001 with the U.S. Department of Energy.

## BACKGROUND

DOP-26 iridium alloy containing nominally 0.3 weight percent tungsten, 60 ppm thorium and 50 ppm aluminum was developed by Oak Ridge National Laboratory (ORNL) for cladding radioactive fuel in radioisotope thermoelectric generators.[1] The thorium and aluminum were added to produce adequate high-temperature impact ductility.[2] Thorium content had to be limited to 60 ±30 ppm because concentrations higher than 100 ppm caused weld-metal cracking during gas tungsten arc welding.[3] This type of cracking has been attributed to solidification cracking and heat-affected zone (HAZ) liquation cracking related to "eutectic patches" on welded alloy grain boundaries. Weld-metal cracking has not been a problem during PuFF Facility welding of DOP-26 iridium alloy clad vent sets.

The solid-solubility of thorium in iridium is very low, probably less than 20 ppm. Thus, thorium at 60 ppm is expected to segregate forming $ThIr_5$ (melting point = 2260°C) containing 19.4 weight percent thorium and/or Ir-$ThIr_5$ eutectic (eutectic temperature = 2080°C) containing ~13 weight percent thorium.[4] Thorium has been shown to segregate to grain boundaries in iridium alloy.[5] Aluminum has also been reported to be inhomogeneously distributed in the alloy.[1] Two impurity elements, calcium and carbon, also segregate in the alloy.

## EXPERIMENTAL

Specimens of DOP-26 iridium alloy clad vent sets welded in the SRP PuFF Facility were examined with a contained SEM at SRL. Specimens free of plutonium-238 contamination were welded on equipment at the SRP Equipment Engineering Department (EED) similar to the PuFF Facility welder (Table 1). These specimens were analyzed at SRL using SEM/XES, EMPA and SAM and at ORNL using a high-resolution SAM or SUPER SAM (Table 2). Grain boundaries in various weld areas were exposed by fracturing the specimens at room temperature. Sometimes both fracture surfaces were analyzed by SEM/XES and EMPA to get complete characterizations of grain boundary features.

## RESULTS

### Weld Quench Area Cracking

Figure 1 shows cracks that formed on the inside surface of the weld quench area on CVS 44 welded in the PuFF Facility. These cracks occur along grain boundaries in alloy welded on the first weld pass and are just ahead of the line where full weld penetration ceased in the region where the gas tungsten arc was quenched.

Figure 2 shows the structure of the weld quench region revealed by fracturing the specimen along the weld centerline. High-magnification examinations of grain boundaries in the single pass weld area of the quench revealed ridge network structures that were not present on grain boundaries in other areas of the weld (Figure 3). Ridge networks were also detected on grain boundaries of small cracks in unwelded alloy adjacent to welds (Figure 4). These observations indicate that the ridge network structure and weld quench area cracking occur in the heat affected zones of welds in DOP-26 alloy.

## Surface Studies

Grain boundary structures and compositions of specimens from DOP-26 alloy clad vent sets welded by SRP EED were analyzed to determine the cause of weld quench cracking. Results for unwelded alloy, welded alloy, the heat-affected zone in the single pass weld area, and large crack surfaces are presented.

### Unwelded Alloy

DOP-26 iridium alloy in the clad vent sets consists of faceted grains about 100 μm in size (Figure 5). Grains are frequently elongated parallel to the cup surfaces. Grain facets are generally smooth with few irregularities. Thorium-bearing particles embedded in the facets are highly dispersed. Occasional thorium-bearing stringers are detected. EMPA indicated thorium concentrations up to 8 wt % and possible traces of copper (Table 4). Thorium concentrations at other points of unwelded grain facets were less than the detection limit of ~0.1 wt %. SUPER SAM analyses at points on unwelded alloy grains showed Th/Ir $\leq$0.25 (Table 5). No elements besides iridium and thorium were detected in these SUPER SAM analyses. Elemental depth profiling of a fracture surface in unwelded alloy with the SAM showed the thorium signal to decrease to below the detection limit (Th/Ir $\approx$0.02) after a few minutes of argon ion sputtering (Figure 6). Such a profile is consistent with this thorium-bearing material being only a few atom layers thick.

### Welded Alloy

Welding not only increases the size of the DOP-26 iridium alloy grains, but it introduces pores within the grains and pores and thorium-bearing particles, stringers and patches onto the grain surfaces (Figures 7-11). When specimens were fractured for analysis, the thorium-bearing features remaining on one surface left similarly shaped depressions on the mating surface whereas pores

produced mating circular depressions. Pores were surrounded by rims where mating grain surfaces made contact. No thorium was detected by SEM/XES in the pores or rims but was detected in the particles, stringers, and patches outside the rims. The pores and thorium-bearing particles and stringers generally formed lines parallel to the welded grain edges. These lines were more closely spaced on grain surfaces in the overlap region of the girth weld where the alloy was welded twice. The thorium-bearing patches and stringers appear to be a few tenths of a micron thick and some have eutectic-like structures (Figure 9). SUPER SAM analyses at points on grain surfaces in the single pass weld region detected only iridium and thorium with Th/Ir $\leq$0.34 (Table 6). SAM thorium depth profiles for grain surfaces in the single pass weld area were nearly identical to those recorded for unwelded alloy and indicated that the surface material is only a few atom layers thick (Figure 6).

### Heat-Affected Zone in the Single Pass Weld Area

Grains in the heat-affected zone of the single pass weld area in the quench region of girth welds are shaped like those in single pass weld areas away from the quench region. Grain surfaces in this heat-affected zone exhibit small pores and thorium-bearing features like those present in other weld areas. However, two types of grain surface depressions have been detected that are not present in other weld areas.

Areas near grain edges (intersections of grain faces) have elongated, irregularly shaped depressions where circular pores seemed to have coalesced (Figures 12-14). These depressed areas are surrounded by distinct rims where mating grain faces made contact. No thorium was detected by SEM/XES or EMPA in the depressions or in the rims. Thorium-bearing patches were detected outside the rims. SUPER SAM analyses of a grain-edge depression area detected only iridium and thorium with Th/Ir = 0.15-0.24 in the depression compared to Th/Ir $\leq$0.14 outside the depression (Figure 14 and Table 7).

Small ridge network structures several microns across and covering only portions of a grain face were detected in the heat-affected zone of the weld quench area of clad vent sets (Figures 15-17). Examinations of mating fracture surfaces showed that ridge patterns on adjoining grain faces are mirror images of each other. Areas between the ridges on both surfaces are recessed a few tenths of a micron and, thus, constitute mating depressions in the grain surfaces. The depressions have smooth, almost mirror-like surfaces compared to rougher grain surfaces outside the ridge networks. In general, ridges are more closely spaced near the edges of the networks. Elemental mapping by EMPA and point analyses by SEM/XES and EMPA failed to detect any thorium in the ridges or in the surfaces of the depressions (Tables 8 and 9).

SUPER SAM analysis of a small ridge network (Figures 17 and 18 and Table 10) detected carbon (C/Ir ≈0.1), as well as thorium (Th/Ir ≈0.4) on surfaces of the voids. Calcium (Ca/Ir ≈0.05) was detected on a ridge. Sputtering for five minutes reduced the signals from thorium and calcium to below the detection limits. Thus, the surface material on the ridge network appears to be only a few atom layers thick.

Thorium-bearing patches several microns across and a few tenths of a micron thick were detected by EMPA mapping (Figures 15 and 16). These patches are generally larger than those detected in other weld areas. Some of these patches adjoin the ridge networks. Point analyses indicate thorium concentrations up to ≈6 wt % (Tables 8 and 9). When specimens were fractured for analysis, portions of this thorium-bearing patch remained with each surface creating raised areas where it was present and matching depressions where it was removed from the mating grain facet. Point 6 in Figure 17 corresponds to a thorium-bearing patch detected by EMPA mapping after SUPER SAM analysis. The result of the SUPER SAM analysis of this point after 5 minutes of sputtering indicated Th/Ir = 0.07 which is consistent with a thorium concentration in this patch of 8.3 wt %.

### Surfaces of Large Cracks in the Weld Quench Area

Figure 19 shows a large crack in the weld quench area on CVS T36 that extends from the heat-affected zone in the single pass weld area into the heat-affected zone in the unwelded alloy at the edge of the weld. Fracturing the specimen along the crack revealed an area consisting of many grains covered by ridge networks extending half way through the 0.70-mm-thick alloy cup (Figures 20 and 21). In general, no thorium was detected by SEM/XES and EMPA in the ridges or depressions between the ridges. However, submicron thorium-bearing particles were detected embedded in the ridges and depressions between the ridges. No thorium-bearing patches were detected in this extended ridge network structure.

In a severely cracked weld quench area on CVS T39, ridge networks covering many grains were detected extending into the columnar grain region (Figure 22). Metallographic examinations of severely cracked weld quench areas have shown that large cracks sometimes extend into the columnar grain region. No thorium was detected by SEM/XES or EMPA in the ridges or depressions between the ridges. Micron-size thorium-bearing particles were detected attached to some of the ridges (Figures 23 and 24). EMPA of one particle indicated a thorium concentration of 9.8 wt %. No other elements besides iridium and thorium were detected in SEM/XES analysis of the particles. Some thorium-bearing patches containing 1.1-1.7 wt % thorium were also present.

## DISCUSSION

### General Interpretations

The ridge network structure is thought to be a characteristic of cracks that form in the quench area of girth welds on DOP-26 iridium alloy clad vent sets. The observation that these cracks are in the heat-affected zones in both welded and unwelded alloy indicates that the mechanism that causes cracking occurs below the melting point of the alloy. The segregation of thorium to alloy grain boundaries has been confirmed by a variety of analytical techniques.

### Interpretations in Terms of Specific Cracking Mechanisms

The analytical results have been interpreted in terms of two mechanisms that could cause cracking in the weld quench area of clad vent set girth welds:

1. Release of gas to alloy grain surfaces which produces several types of porosity including the extended ridge networks which weaken grain boundaries and cause cracking because of welding stresses.

2. Liquation on grain surfaces which weakens them, causes cracking because of welding stresses, and produces the ridge networks.

The author is a proponent of the gas porosity mechanism.

### Interpretations in Terms of Gas Porosity

The following interpretations of analytical results support the concept that grain boundary gas porosity is the cause of weld quench area cracking: (1) the pores within welded grains; (2) the small pores on grain surfaces of welded alloy; (3) the elongated depressions at grain edges and small ridge networks on grain faces in the heat-affected zone of the single pass weld; and (4) the extended ridge networks covering many grains on surfaces of large cracks are all interpreted as gas porosity caused by release of increasing amounts of gas from the alloy on heating to near the melting point. These forms of grain boundary porosity have several structural similarities. The depressions correspond to areas where grain surfaces have deformed to accommodate the gas. Adjacent grain surfaces make contact along the rims and ridges. No thorium has been detected in the rims, ridges, or depressions. Smooth surfaces like those observed in grain edge porosity and ridge network porosity are a characteristic of gas porosity.[6] The

observation that small ridge networks often form near the center of grain faces (Figure 17) is consistent with them being formed by gas pressurization rather than a mechanism related to grain boundary separation. The observation that the spacing between ridges increases from the edge to the center of the networks indicates that the depth is greater near the center as would be expected for gas porosity.

Porosity caused by release of gas to grain surfaces on heating to temperatures significantly below the melting point has been observed in metals and ceramics. Ridge networks in DOP-26 iridium alloy are striking similar to porosity in $^{238}PuO_2$ caused by helium from alpha decay being released to grain surfaces on heating to 1700°C.[7] This porosity in $^{238}PuO_2$ consists of circular pores which coalesce to form elongated conduits on grain triple lines (similar to grain edge porosity) and irregular shaped depressions with curved edges on grain faces (similar to ridge networks). DOP-26 iridium alloy, because of its brittle nature, is expected to respond to gas released to grain boundaries in a manner similar to a ceramic rather than a ductile metal.

High-magnification examination of a polished cross section through CVS weld quench areas at Los Alamos National Laboratory (LANL) revealed bubbles and grain separations in grain boundaries in heat-affected zones in the single pass weld area and unwelded alloy that were attributed to gas porosity.[8] These areas containing porosity are the same ones where ridge network porosity has been detected on fracture surfaces. Gas porosity in the form of large blisters has been observed in DOP-26 iridium alloy sheet heated to 2000°C for one hour.[9] Gas voids also have been observed in DOP-26 alloy ingots.[10]

Grain boundary gas porosity in both metals and ceramics can form in the absence of grain boundary liquation. The failure of SEM/XES and EMPA to detect any elements that could form low-melting phases or eutectics in rims, ridges, and depressions in grain edge porosity and ridge networks supports the contention that liquation is not needed for these features to form. The observation of ridge networks on facets of unwelded grains, which have been shown to have very little surface thorium provides further support. The thorium-bearing particles detected in extended networks on large crack surfaces are thought to be ones that formed on these surfaces during the first weld pass and followed the rest of the surface during the deformation caused by gas pressurization. The presence of thorium-bearing particles on ridges in the columnar grains in CVS T39 can be explained by the ridge networks forming in areas away from these particles and growing until the particles are surrounded. It must be noted that the thorium-bearing patches, which are areas that would be expected to be most likely to undergo liquation, do not have the ridge network structure.

The SAM results for the points in the small ridge network in Figure 17 are interpreted as evidence of gas within the porosity that adsorbed on or reacted with the pore surface. These SAM results are consistent with the gas being hydrogen, helium or a hydrocarbon but not an oxygen-bearing gas like $H_2O$, CO, $CO_2$ or $IrO_2$. Hydrogen is used in arc casting of the DOP-26 alloy. Helium is used in both alloy preparation and welding. A hydrocarbon could be formed by reaction between carbon impurity in the alloy and hydrogen or moisture in process gases. Specifically, a reaction between calcium carbide and moisture would produce acetylene. Since the thickness of this surface material is so small ($\sim 1 \times 10^{-8}$m) compared to the separation between grains in the porosity regions ($\sim 1 \times 10^{-6}$m), it is considered unlikely that this surface material plays a significant role in cracking.

Weld quench cracking is a form of underbead cracking in heat-affected zones rather than the weld-metal cracking in iridium alloys studied by ORNL.[3] Therefore, it seems likely that a mechanism like grain boundary gas porosity, which is different from grain boundary liquation which causes weld-metal cracking, could be the cause of weld quench cracking. The observation that the ridge network structure characteristic of weld quench area cracking is distinctly different from that of the "eutectic patches" associated with weld-metal cracking supports the contention that these are two different types of cracking caused by two different mechanisms.

### Interpretations in Terms of Grain Boundary Liquation

The following interpretations of analytical results support the concept that grain boundary liquation causes weld quench area cracking in girth welds in DOP-26 iridium alloy clad vent sets, and that the ridge networks are evidence of this liquation.

The grain edge depressions and ridge networks have the appearance of melted material. These features are interpreted as an eutectic-like phase with dendritic structure. The presence of this phase on surfaces of unmelted alloy grains beyond the weld penetration depth is evidence that the melting point of this phase is below that of the iridium alloy. The detection of thorium in the ridge networks on CVS's T36 and T39 indicates an eutectic phase.

Grain boundary liquation could lead to formation of the ridge network structure in several ways. The ridges could be formed as the molten eutectic phase is pulled apart during grain separation caused by welding stresses. Alternately, molten material between the ridges could flow out into the grain boundaries under surface tension or capillary action leaving the depressions. The smooth surfaces of these depressions are thought to be characteristic of a

solidified liquid phase. The SAM results for points in a small ridge network (Figures 17 and 18 and Table 10) are interpreted as evidence of a low-melting phase or eutectic that is not present on grain boundaries outside the ridge network.

Weld quench area cracking in DOP-26 alloy is thought to be caused by the same mechanism that causes weld-metal cracking. Liquation cracking in the heat-affected zone could explain the formation of weld quench area cracks.

ACKNOWLEDGEMENT

The support of P. G. Whitkop of SRL and C. L. White of ORNL in performing the AES analyses is appreciated. F. W. Schonfeld of LANL kindly provided results of metallographic examinations showing gas porosity in heat-affected zones of CVS welds. E. F. Sturcken of SRL performed SEM/XES analyses to confirm observations by the author. The assistance of E. F. Sturcken along with W. R. Kanne, J. D. Scarbrough and B. K. Roberts of SRP in providing arguments supporting the grain boundary liquation explanation of weld quench area cracking is acknowledged.

REFERENCES


1. H. Inouye. "Platinum Group Alloy Containers for Radioisotopic Heat Sources," **Platinum Metals Review, 23,** 100-107 (July 1979).

2. C. T. Liu, H. Inouye and C. A. Schaffhauser, "Effect of Thorium Additions on Metallurgical and Mechanical Properties of Ir - 0.3 Pct W Alloys," **Metallurgical Transactions A, 12A,** 993-1002 (June 1981).

3. S. A. David and C. T. Liu. **Weldability and Hot Cracking in Thorium-Doped Iridium Alloys, Metal Technology,** 102-106 (March 1989).

4. W. G. Moffatt, **The Handbook of Binary Phase Diagrams, Vol. 3.** Published by the General Electric Co., Schenectady, NY, (1981).

5. Calvin L. White, Robert E. Clausing, and Lee Heatherly. "The Effect of Trace Element Additions on the Grain Boundary Composition of Ir + 0.3 Pct W Alloys." **Metallurgical Transactions A, 10A,** 683-691 (June 1979).

6. Howard E. Boyer, editor. **Metal Handbook, 8th Edition, Vol. 9** "Fractography and Atlas of Fractographs." 100-101, published by the American Society of Metals, Metals Park, OH (1974).

7. General-Purpose Heat Source Project and Space Nuclear Safety and Fuels Program, August 1980 Report, LA-8713-PR.

8. **Space Nuclear Safety and Fuels Program, December 1981.** LA-9311-PR.

9. **Technical Highlights of Space and Terrestrial Systems Programs at Oak Ridge National Laboratory for December 1980.** ORNL/CF-81/34.

10. **Technical Highlights of Space and Terrestrial Systems Programs at Oak Ridge National Laboratory for February 1981.** ORNL/CF-81-60.

TABLE 1

Specimens Used in DOP-26 Iridium Alloy Weld-Quench Cracking Studies

| CVS Number* | Description | Analysis Methods |
|---|---|---|
| 44 | Weld-Quench Crack | CSEM |
| 67 | Weld-Quench Crack | CSEM |
| 84 | Crack in Vent Hole Weld-Quench | CSEM |
| 85 | Crack near Weld Shield Contact | CSEM |
| MHW 101 | Weld-Quench in Post Impact Containment Shell | SEM, EMPA, SAM, SSMS |
| T2 | Ouench, Crack at Weld Edge | SEM/XES, EMPA, SAM, SUPER SAM, SSMS |
| T10 | Cracks in Quench in Unwelded Alloy | SEM |
| T20 | Single Pass Weld | SEM |
| T24 | Single Pass Weld | SEM |
| T25 | Cracks in Long Taper Quench | SEM |
| T29 | Single Pass Weld | SEM, SIMS |
| T36 | Cracks in Long Taper Quench | SEM/XES, EMPA, SUPER SAM, SSMS |
| T37 | Multiple Quenches (NR Cups) | SEM |
| T38 | Multiple Quenches (LR Cups) | SEM/XES, SIMS SSMS |
| T39 | Multiple Quenches (MER Cups) | SEM/XES, EMPA, SIMS, SSMS |
| T41 | Long Taper Ouench (MERR Cups) | SEM/XES, SIMS |

* CVS's with T prefix welded by SRP-EED. Others welded in the PuFF Facility.

TABLE 2

Instrumentation Used in DOP-26 Iridium Alloy Weld Quench Cracking Studies

| Technique | Instrument | Description |
|---|---|---|
| CSEM | Cambridge Stereascan 600 | Resolution: ~2.5 x $10^{-8}$m (250Å) |
| SEM/XES | AMR Model 900 | Resolution: ~2.5 x $10^{-8}$m(250Å)<br>Analysis Depth: 2 x $10^{-7}$m(0.2 μm)<br>Elements: Z ≥9<br>Detection Limit: 1 w/o Th |
| AES | Perkin Elmer Model 545 Scanning Auger Microprobe (SAM) | Resolution: 1 x $10^{-5}$m (10 μm)<br>Analysis Depth: ~1 x $10^{-9}$m (10Å)<br>Elements: Z ≥3<br>Detection Limit: 2 w/o Th |
| | Perkins Elmer Model 590 Scanning Auger Microprobe at ORNL (SUPER SAM) | Resolution: 2 x $10^{-7}$m (0.2 μm)<br>Analysis Depth: 1 x $10^{-9}$m (10Å)<br>Elements: Z ≥3<br>Detection Limit: 2 w/o Th |
| EMPA | Applied Research Laboratories Scanning Electron Microprobe Quantometer (SEMQ) | Resolution: 2 x $10^{-7}$m (0.2 μm)<br>Analysis Depth: 3 x $10^{-7}$m (0.3 μm)<br>Elements: Z ≥5<br>Detection Limit: 0.1 w/o Th for points<br>0.5 w/o Th for maps |
| SIMS | Cameca Ion Microscopes at Charles Evans and Associates, San Mateo, California | Resolution: 3 x $10^{-7}$m (0.3 μm)<br>Analysis Depth: 0.3-3 x $10^{-6}$m (0.3-3 μm)<br>Elements: All except noble gases.<br>Detection Limit: ~1 ppb Th |

TABLE 3

EMPA Results* for Bulk DOP-26 Iridium Alloy and an Iridium Standard

| Element | Polished DOP-26 Alloy | | Transgranular Fracture Surfaces of DOP-26 Grains Near Weld Centerline | | Iridium Standard |
|---|---|---|---|---|---|
| Ir | 99.64 | 99.45 | 99.51 | 99.60 | 99.81 |
| W | 0.30 | 0.30 | 0.42 | 0.31 | 0.00 |
| Th | 0.02 | 0.00 | 0.02 | 0.09 | 0.00 |
| Cr | 0.00 | 0.00 | 0.00 | 0.00 | 0.00 |
| Fe | 0.01 | 0.00 | 0.00 | 0.00 | 0.01 |
| Ni | 0.01 | 0.00 | 0.00 | 0.00 | 0.01 |
| Cu | 0.02 | 0.23 | 0.00 | 0.00 | 0.10 |
| Si | 0.01 | 0.01 | 0.01 | 0.00 | 0.01 |
| P | 0.00 | 0.00 | 0.00 | 0.00 | 0.00 |
| S | 0.01 | 0.01 | 0.01 | 0.00 | 0.00 |
| Mo | 0.00 | 0.00 | 0.03 | 0.00 | 0.06 |
| Ag | 0.00 | 0.00 | 0.00 | 0.00 | 0.00 |
| Al | 0.00 | 0.00 | † | † | 0.00 |

* Elemental concentrations in weight percent normalized to 100%

† Not measured

TABLE 4

EMPA Results* for Grain Surfaces in Unwelded Alloy in CVS T2

| | Intergranular Fracture Surfaces of Unwelded Grains | | |
|---|---|---|---|
| Element | Grain Surfaces | | Particle in Stringer |
| Ir | 99.35 | 99.55 | 91.34 |
| W | 0.57 | 0.38 | 0.19 |
| Th | 0.00 | 0.05 | 7.99 |
| Cr | 0.00 | 0.00 | 0.00 |
| Fe | 0.01 | 0.00 | 0.00 |
| Ni | 0.00 | 0.00 | 0.01 |
| Cu | 0.02 | 0.00 | 0.12 |
| Si | 0.00 | 0.00 | 0.00 |
| P | 0.00 | 0.00 | 0.00 |
| S | 0.01 | 0.01 | 0.00 |
| Mo | 0.05 | 0.00 | 0.01 |
| Ag | 0.00 | 0.00 | 0.30** |
| Al | † | † | † |

* Elemental concentrations in weight percent normalized to 100%

** Interference from Thorium Mα x-ray

† Not measured

TABLE 5

**Results of SUPER SAM Analysis of a Unwelded Alloy Specimen from CVS No. T2**

| Analysis Point No. | Area 1 | Auger Peak Intensity Ratio* Th (67 eV) / Ir (54 eV) | Estimated Atom Fractions Ir | Th |
|---|---|---|---|---|
| 1 | Fractured Grain | 0.05 | 0.95 | 0.05 |
| 2 | Grain Boundaries | 0.17 | 0.86 | 0.14 |
| 3 | | 0.25 | 0.80 | 0.20 |
| | Area 2 | | | |
| 1 | Fractured Grain | 0.05 | 0.95 | 0.05 |
| 2 | Grain Boundaries | 0.13 | 0.88 | 0.12 |
| 3 | | 0.25 | 0.80 | 0.20 |

* Only Ir and Th detected

TABLE 6

Results of SUPER SAM Analysis of a Single-Pass Weld Specimen from CVS No. T2

| Analysis Point No. | Area 1 | Auger Peak Intensity Ratio* Th (67 eV) / Ir (54 eV) | Auger Peak Intensity Ratio* C (272 eV) / Ir (229 eV) | Estimated Atom Fractions Ir | Th | C |
|---|---|---|---|---|---|---|
| 1 | Grain Boundary | 0.18 | <.3 | 0.85 | 0.15 | 0.0 |
| 2 | Fractured Grain | 0.04 | <.3 | 0.97 | 0.03 | 0.0 |
| 3 | Grain Boundary | 0.20 | <.3 | 0.84 | 0.16 | 0.0 |
| | Area 2 | | | | | |
| 1 | | 0.12 | <.3 | 0.89 | 0.11 | 0.0 |
| 2 | | 0.23 | <.3 | 0.81 | 0.19 | 0.0 |
| 3 } | Grain Boundaries | 0.34 | <.3 | 0.75 | 0.25 | 0.0 |
| 4 | | 0.19 | <.3 | 0.84 | 0.16 | 0.0 |
| 5 | | 0.18 | <.3 | 0.85 | 0.15 | 0.0 |
| 6 | | 0.25 | <.3 | 0.80 | 0.20 | 0.0 |
| | Area 3 | | | | | |
| | After Sputtering 5 minutes | | | | | |
| 1 | | <.02 | 1.29† | 0.70 | 0.00 | 0.30† |
| 2 } | Grain Boundaries | <.02 | 1.00† | 0.75 | 0.00 | 0.25† |

* Peaks reported as < were not detected

† Carbon probably introduced by sputtering

TABLE 7

Results of SUPER SAM Analysis of Points near A Grain-Edge Depression on Grain Surfaces in the Heat-Affected Zone on CVS T36 (See Figure 14).

| Point Analysis | Location | Auger Peak Intensity Ratios* Th (67 eV) / Ir (54 eV) | C (272 eV) / Ir (229 eV) | O (503 eV) / Ir (229 eV) | Estimated Atom Fractions Ir | Th | C | O |
|---|---|---|---|---|---|---|---|---|
| 1 | Pore | 0.24 | <0.67 | <0.67 | 0.81 | 0.19 | 0.00 | 0.00 |
| 2 | Grain Surface | 0.05 | <0.60 | <0.60 | 0.95 | 0.05 | 0.00 | 0.00 |
| 3 | Pore | 0.18 | <0.36 | <0.36 | 0.85 | 0.15 | 0.00 | 0.00 |
| 4 | Grain Surface | 0.13 | <0.45 | <0.45 | 0.88 | 0.12 | 0.00 | 0.00 |
| 5 | Grain Surface | 0.06 | <0.56 | <0.56 | 0.94 | 0.06 | 0.00 | 0.00 |
| 6 | Pore | 0.22 | <0.60 | <0.60 | 0.82 | 0.18 | 0.00 | 0.00 |
| 7 | Uncertain | 0.21 | 0.24 | 0.69 | 0.65 | 0.13 | 0.00 | 0.22 |
| 8 | Grain Surface | 0.09 | <0.30 | <0.30 | 0.92 | 0.08 | 0.00 | 0.00 |
| 9 | Pore | 0.15 | <0.39 | <0.39 | 0.87 | 0.13 | 0.00 | 0.00 |
| 10 | Grain Surface | 0.12 | <0.33 | <0.33 | 0.89 | 0.11 | 0.00 | 0.00 |
| 11 | Grain Surface | 0.14 | <0.38 | <0.38 | 0.88 | 0.12 | 0.00 | 0.00 |

* Peaks reported as < were not detected.

TABLE 8

EMPA Results* for Points on the Grain Surface with a Small Ridge Network Shown in Figure 15.

| | Points in Ridge Network | | | | | Points Adjacent to Ridge Network | | | | | Points Away from Ridge Network | | |
|---|---|---|---|---|---|---|---|---|---|---|---|---|---|
| | Area Between Ridges | | | Ridges | | | | | | | | | |
| Element | No. 2 | No. 8 | No. 11 | No. 6 | No. 7 | No. 1 | No. 3 | No. 4 | No. 5 | No. 9 | No. 12 | No. 13 | No. 14 |
| Ir | 99.57 | 99.64 | 99.71 | 99.58 | 99.68 | 93.60 | 99.34 | 99.64 | 99.66 | 98.77 | 99.69 | 99.56 | 97.93 |
| W | 0.31 | 0.25 | 0.18 | 0.23 | 0.14 | 0.16 | 0.34 | 0.25 | 0.19 | 0.23 | 0.25 | 0.33 | 0.06 |
| Th | 0.07 | 0.08 | 0.04 | 0.05 | 0.11 | 5.93 | 0.24 | 0.02 | 0.12 | 0.85 | 0.02 | 0.02 | 1.75 |
| Cr | 0.00 | 0.00 | 0.00 | 0.00 | 0.00 | 0.00 | 0.00 | 0.00 | 0.00 | 0.00 | 0.00 | 0.00 | 0.00 |
| Fe | 0.00 | 0.00 | 0.00 | 0.00 | 0.00 | 0.00 | 0.00 | 0.00 | 0.00 | 0.00 | 0.00 | 0.00 | 0.00 |
| Ni | 0.04 | 0.00 | 0.03 | 0.01 | 0.00 | 0.00 | 0.01 | 0.00 | 0.00 | 0.00 | 0.01 | 0.00 | 0.01 |
| Cu | 0.00 | 0.01 | 0.00 | 0.00 | 0.00 | 0.03 | 0.00 | 0.00 | 0.00 | 0.00 | 0.00 | 0.00 | 0.15 |
| Si | 0.01 | 0.01 | 0.02 | 0.04 | 0.02 | 0.03 | 0.02 | 0.02 | 0.03 | 0.06 | 0.02 | 0.01 | 0.02 |
| P | 0.01 | 0.00 | 0.00 | 0.00 | 0.00 | 0.00 | 0.01 | 0.00 | 0.00 | 0.00 | 0.00 | 0.00 | 0.01 |
| S | 0.01 | 0.01 | 0.01 | 0.01 | 0.01 | 0.00 | 0.01 | 0.01 | 0.00 | 0.00 | 0.02 | 0.00 | 0.00 |
| Mo | 0.00 | 0.00 | 0.01 | 0.06 | 0.03 | 0.00 | 0.02 | 0.06 | 0.00 | 0.06 | 0.00 | 0.07 | 0.00 |
| Ag | 0.00 | 0.00 | 0.00 | 0.00 | 0.00 | 0.24** | 0.01 | 0.00 | 0.00 | 0.04** | 0.00 | 0.01 | 0.08** |
| Al | 0.00 | 0.00 | 0.01 | 0.00 | 0.00 | 0.01 | 0.00 | 0.01 | 0.00 | 0.00 | 0.00 | 0.00 | 0.00 |

* Elemental concentrations in weight percent normalized to 100%

** Interference from Thorium M α x-ray

TABLE 9

**EMPA Results* for Points on the Grain Surface with a Small Ridge Network Shown in Figure 16.**

| | Analysis Points in Ridge Network | | | | | | |
|---|---|---|---|---|---|---|---|
| | Ridges | | Area Between Ridges | | | | |
| Element | No. 7 | No. 8 | No. 2 | No. 4 | No. 6 | No. 9 | No. 14 |
| Ir | 99.96 | 99.68 | 99.95 | 99.65 | 99.80 | 99.69 | 99.45 |
| W | 0.02 | 0.28 | 0.00 | 0.31 | 0.14 | 0.28 | 0.51 |
| Th | 0.02 | 0.04 | 0.05 | 0.04 | 0.06 | 0.03 | 0.04 |

| | Analysis Points in Area Around Ridge Network | | | | | | |
|---|---|---|---|---|---|---|---|
| | No. 1 | No. 3 | No. 5 | No. 10 | No. 11 | No. 12 | No. 13 |
| Ir | 96.25 | 96.26 | 97.82 | 96.14 | 99.48 | 98.77 | 99.58 |
| W | 0.05 | 0.24 | 0.07 | 0.19 | 0.50 | 0.08 | 0.06 |
| Th | 3.70 | 3.50 | 2.11 | 3.67 | 0.02 | 1.15 | 0.36 |

* Weight percent

TABLE 10

Results of SUPER SAM Analysis of a Ridge Network on the Quench Specimen from CVS No. T2 (See Figure 17)

| Analysis Point No. | As Fractured | Auger Peak Intensity Ratios* Th (67 eV) / Ir (54 eV) | C (272 eV) / Ir (229 eV) | Ca (29 eV) / Ir (229 eV) | Estimated Atom Fractions Ir | Th | C | Ca |
|---|---|---|---|---|---|---|---|---|
| 1 | Ridge | 0.36 | 0.35 | 0.45 | 0.66 | 0.24 | 0.07 | 0.03 |
| 2 | Points | 0.45 | 0.43 | <0.1 | 0.68 | 0.28 | 0.09 | 0.00 |
| 3 | Between Ridges | 0.42 | 0.43 | <0.1 | 0.64 | 0.27 | 0.09 | 0.00 |
| 4 | Grain Boundary | 0.15 | <0.2 | <0.1 | 0.88 | 0.12 | 0.00 | 0.00 |
| 5 | Outside | 0.22 | <0.2 | <0.1 | 0.83 | 0.17 | 0.00 | 0.00 |
| 6 | Ridge Network | 0.26 | <0.2 | <0.1 | 0.81 | 0.19 | 0.00 | 0.00 |
| | Same Points After Sputtering 5 minutes | | | | | | | |
| 1 | Ridge | <0.02 | 0.80† | <0.1 | 0.79 | 0.00 | 0.21† | 0.00 |
| 2 | Points | <0.02 | 0.72† | <0.1 | 0.81 | 0.00 | 0.19† | 0.00 |
| 3 | Between Ridges | <0.02 | 0.82† | <0.1 | 0.79 | 0.00 | 0.21† | 0.00 |
| 4 | Grain Boundary | <0.02 | 0.86† | <0.1 | 0.79 | 0.00 | 0.21† | 0.00 |
| 5 | Outside | 0.02 | 0.70† | <0.1 | 0.81 | 0.02 | 0.17† | 0.00 |
| 6 | Ridge Network | 0.07 | 0.61† | <0.1 | 0.80 | 0.05 | 0.15† | 0.00 |

* Peaks reported as < were not detected.

† Carbon probably introduced by sputtering.

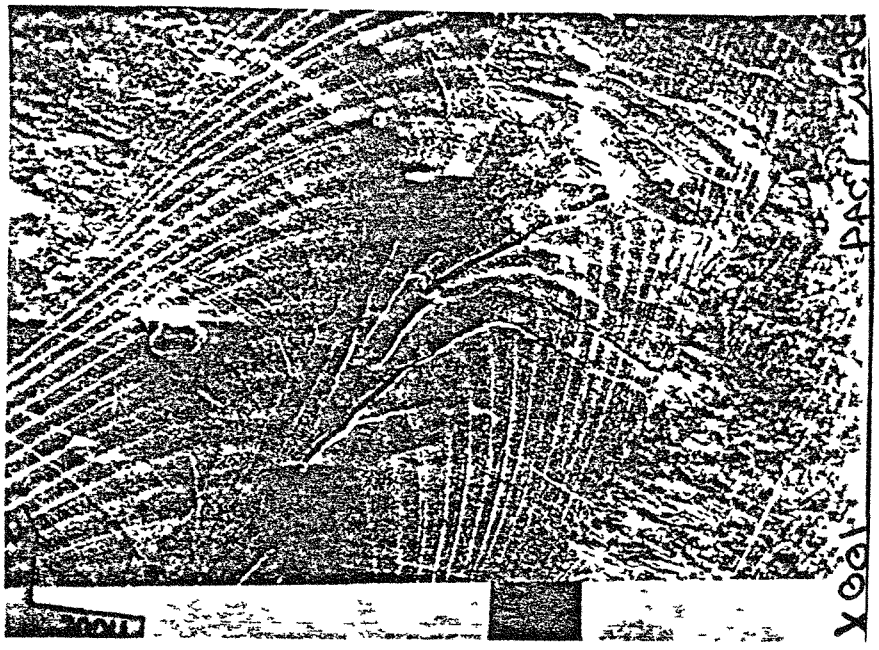

Figure 1. Weld Quench Cracks in Heat-Affected Zone Near Ouench Taper on CVS 67 Welded in the PuFF Facility

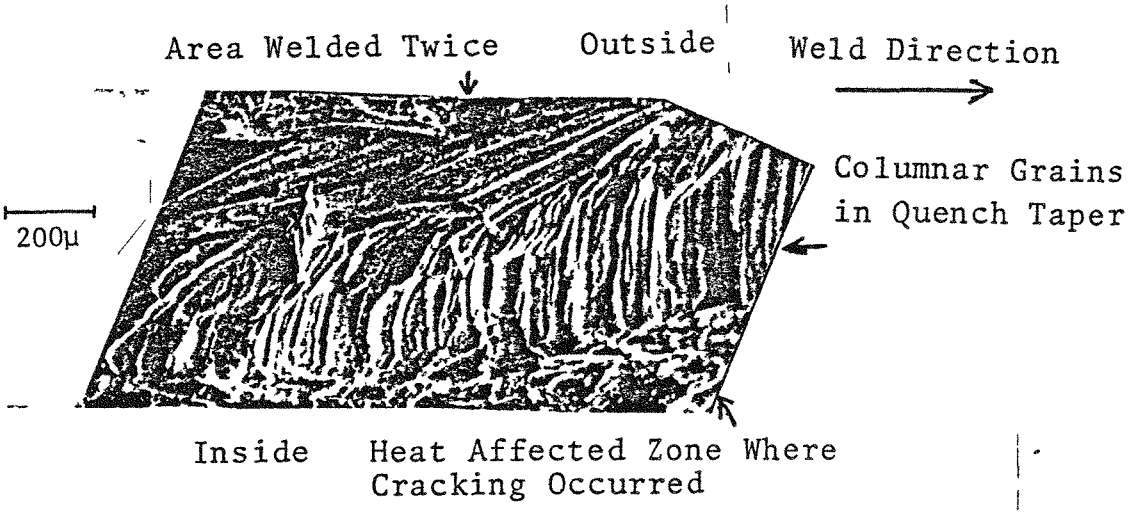


Figure 2. PuFF-Welded CVS 44 Fractured Along Weld Centerline Through Quench

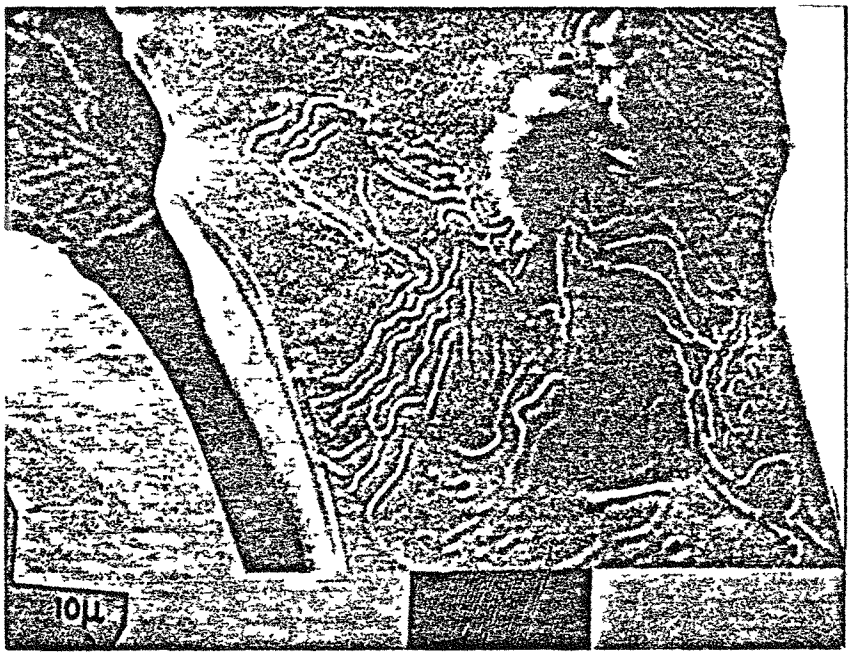


Figure 3. Ridge Networks on Grain Surfaces in Heat-Affected Zone Near Quench Taper on CVS 44

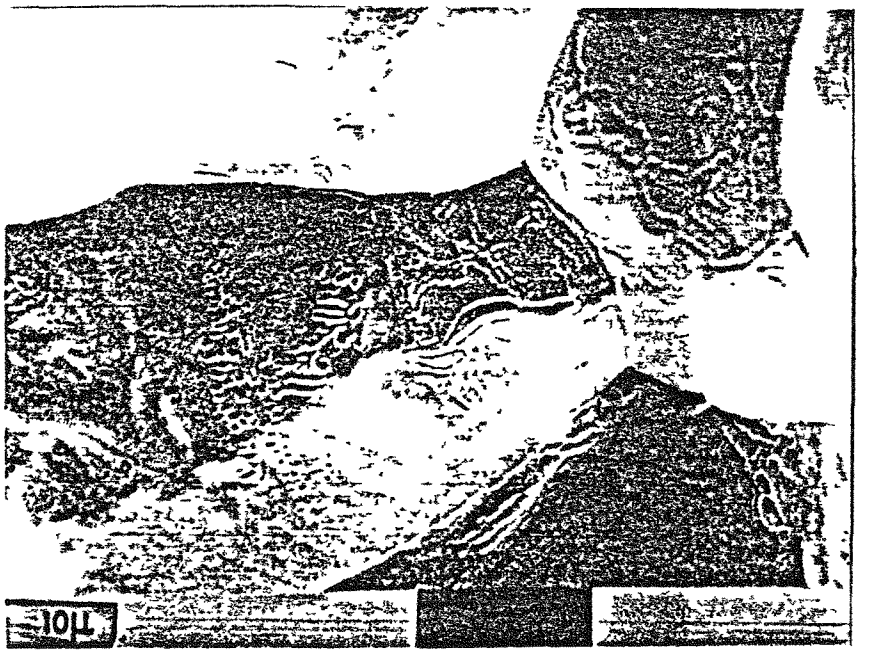


Figure 4. Ridge Network Structures on Unwelded DOP-26 Alloy Grains in Heat-Affected Zone near Weld in CVS

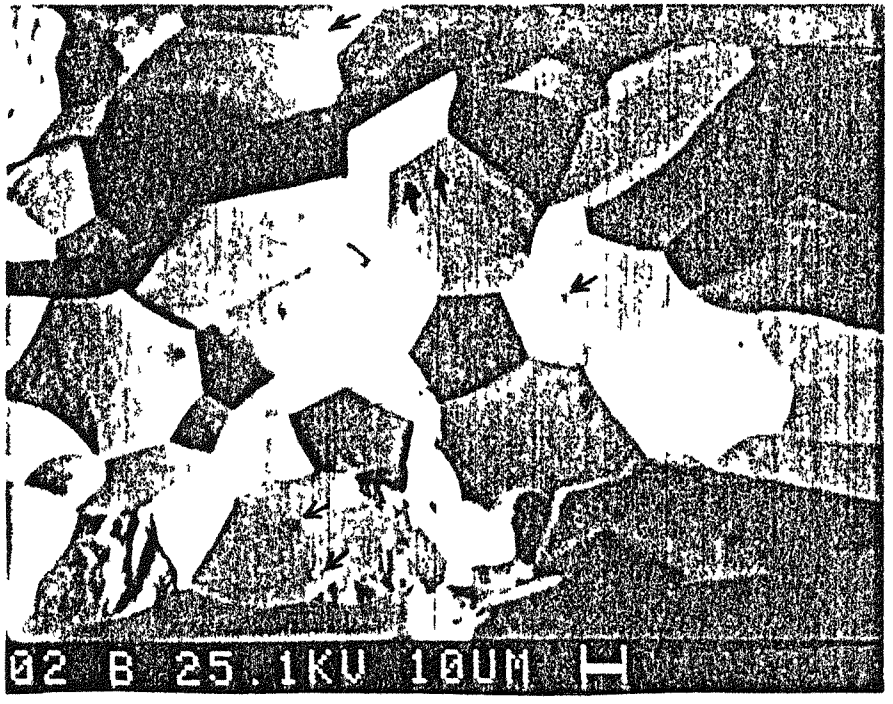


Electron Image

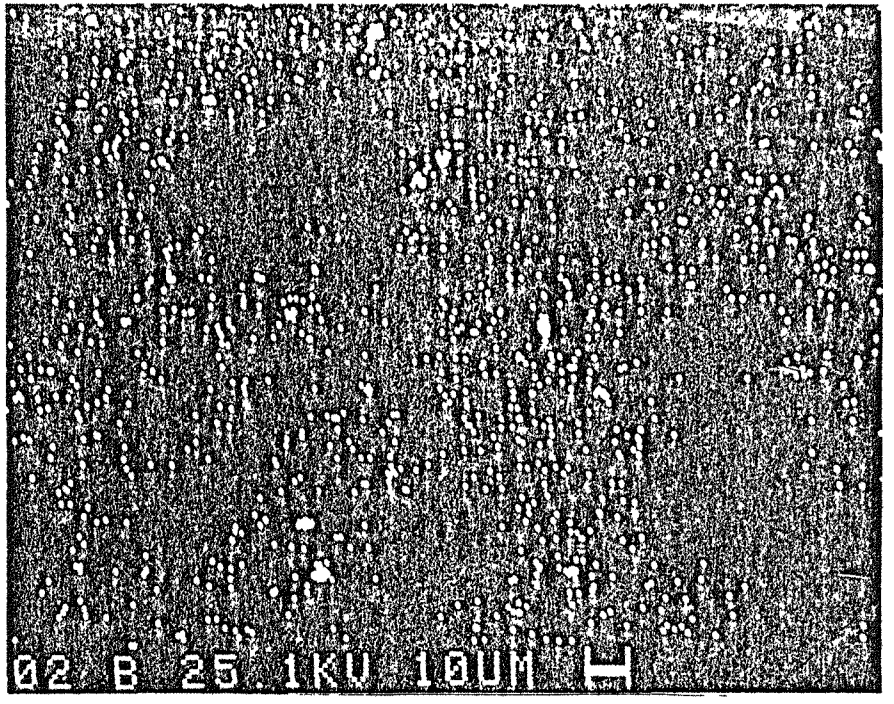


Th Map

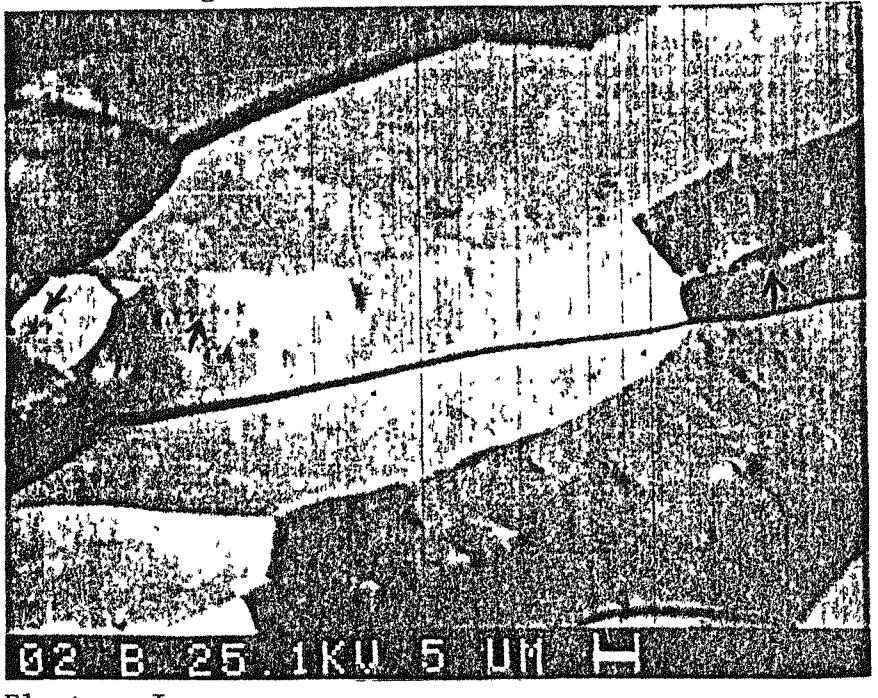


Electron Image

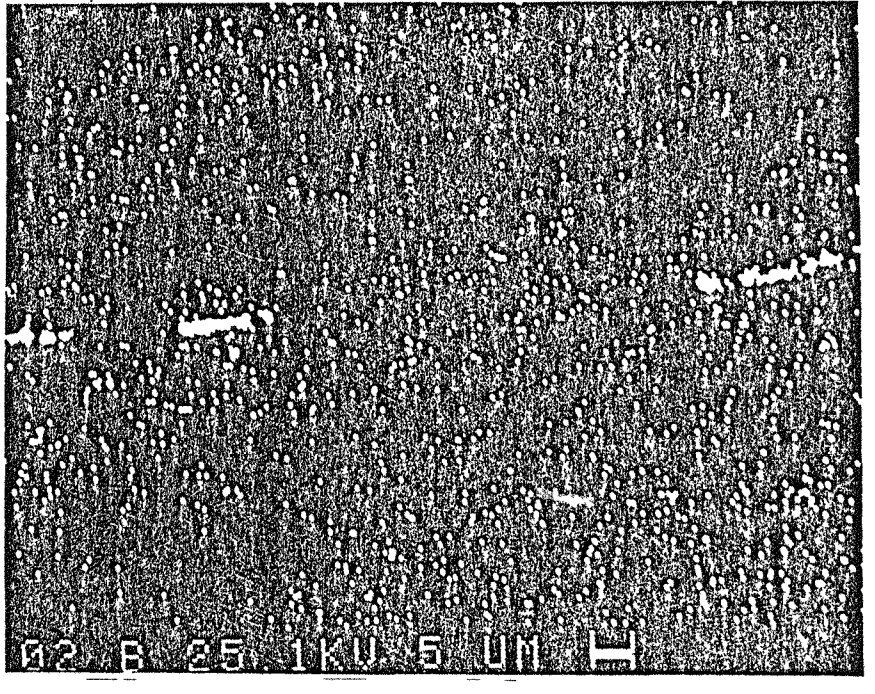


Th Map

Figure 5. EMPA of a Fracture Surface in Unwelded DOP-26 Alloy in CVS T2 Showing Thorium-Bearing Particles (Arrows)

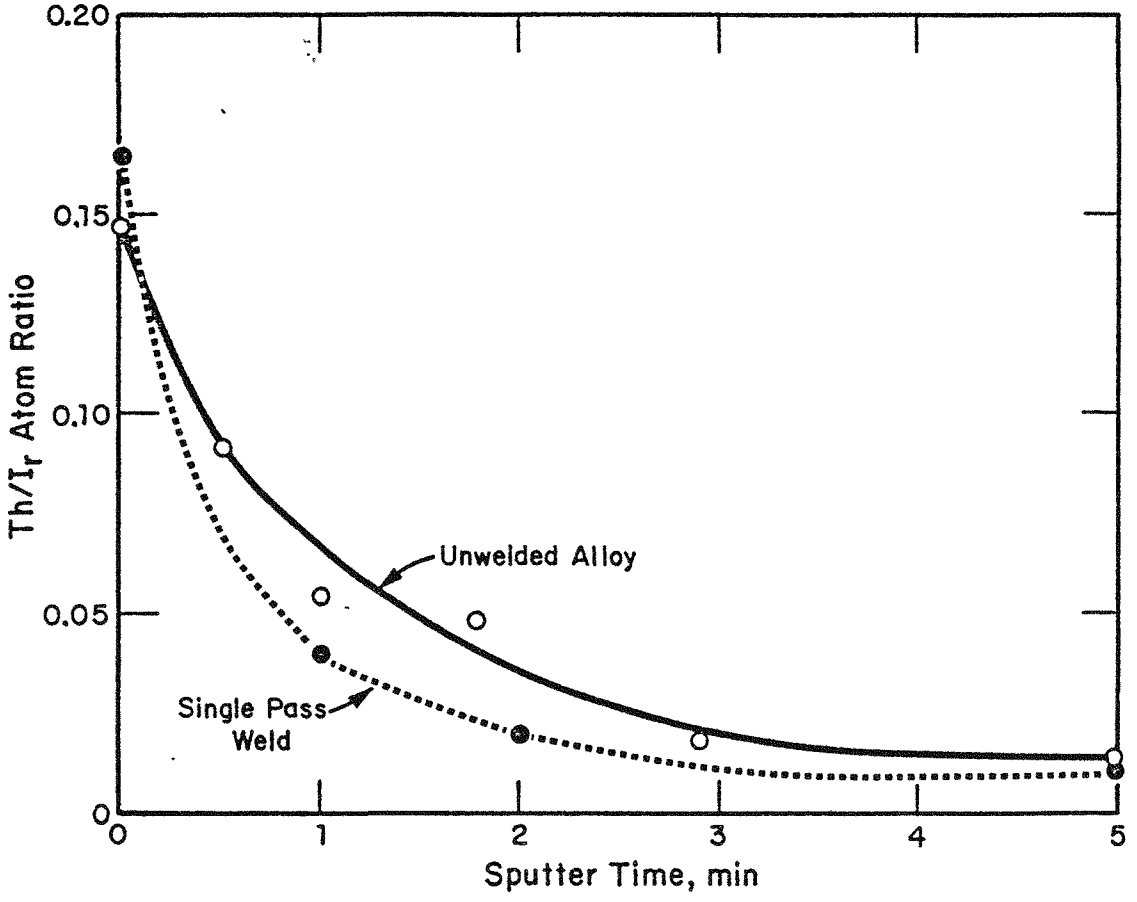


Figure 6. SAM Th/Ir Profiles for DOP-26 Alloy Specimens from MHW PICS 101T.

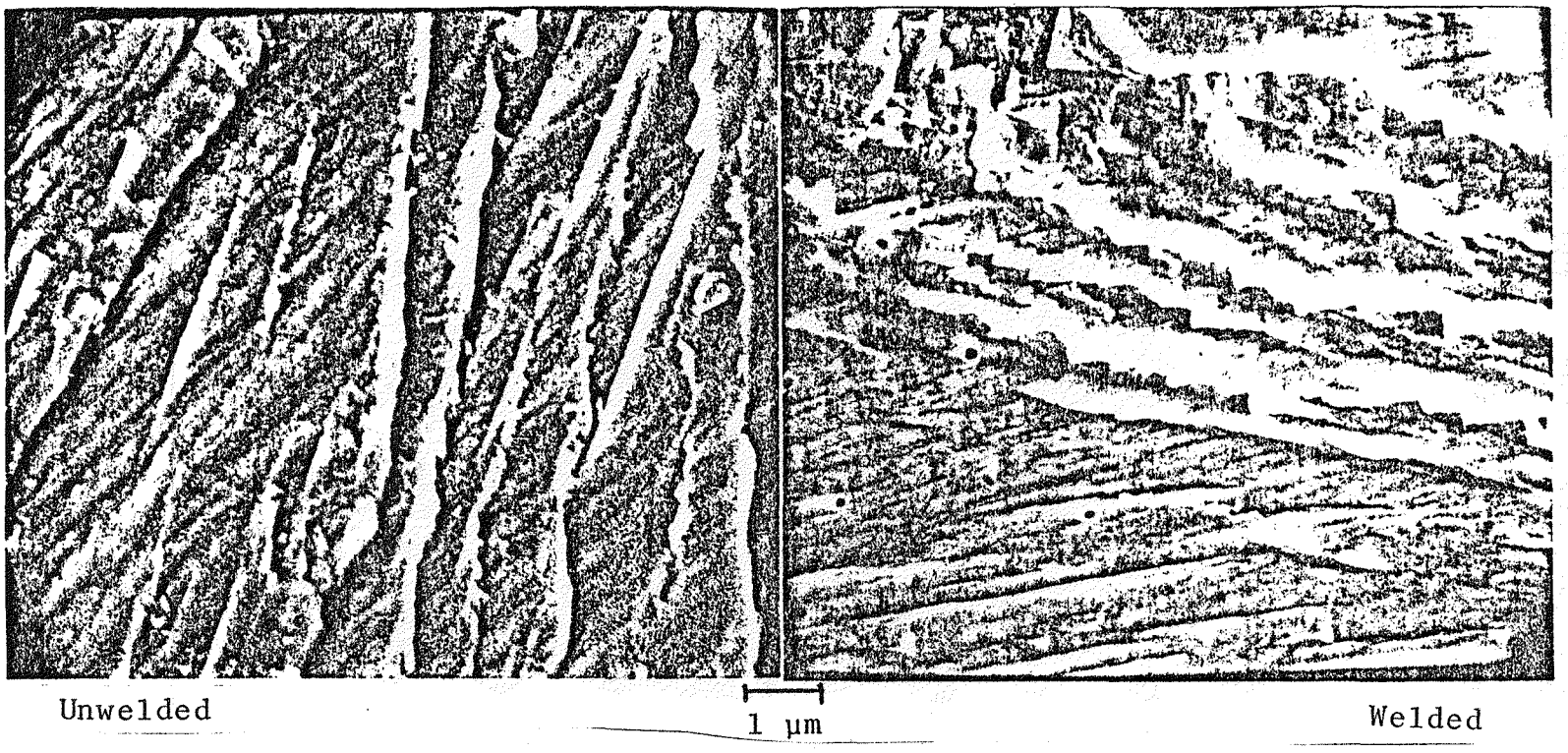


Figure 7. SEM Analyses of Transgranular Fracture Surfaces in Cup MER 5-6 of CVS T39 Showing Porosity Within Welded Alloy Grains but None in Unwelded Alloy

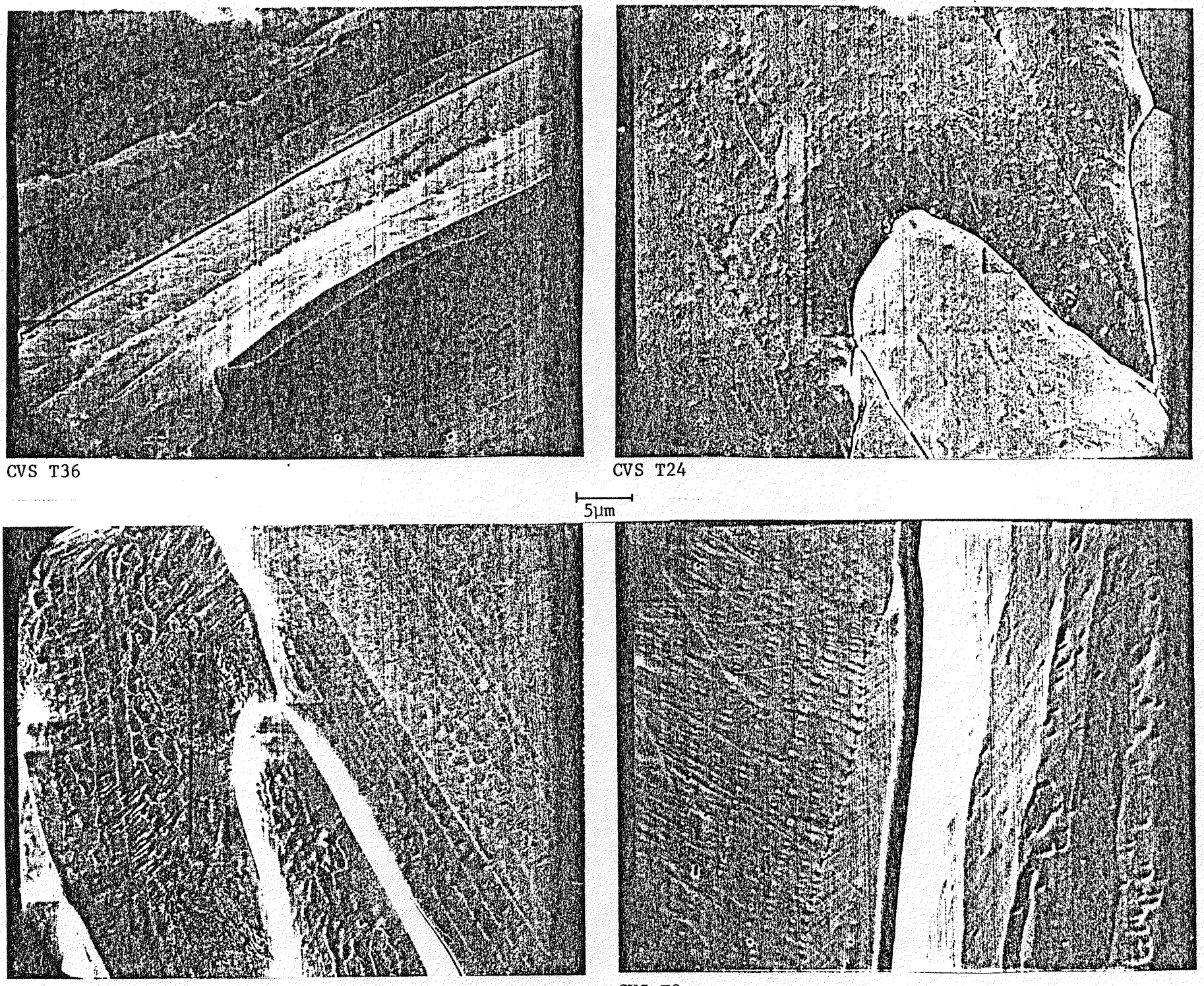


Figure 8. Grain Surfaces in Welded DOP-26 Alloy Showing Pores and Thorium-Bearing Particles

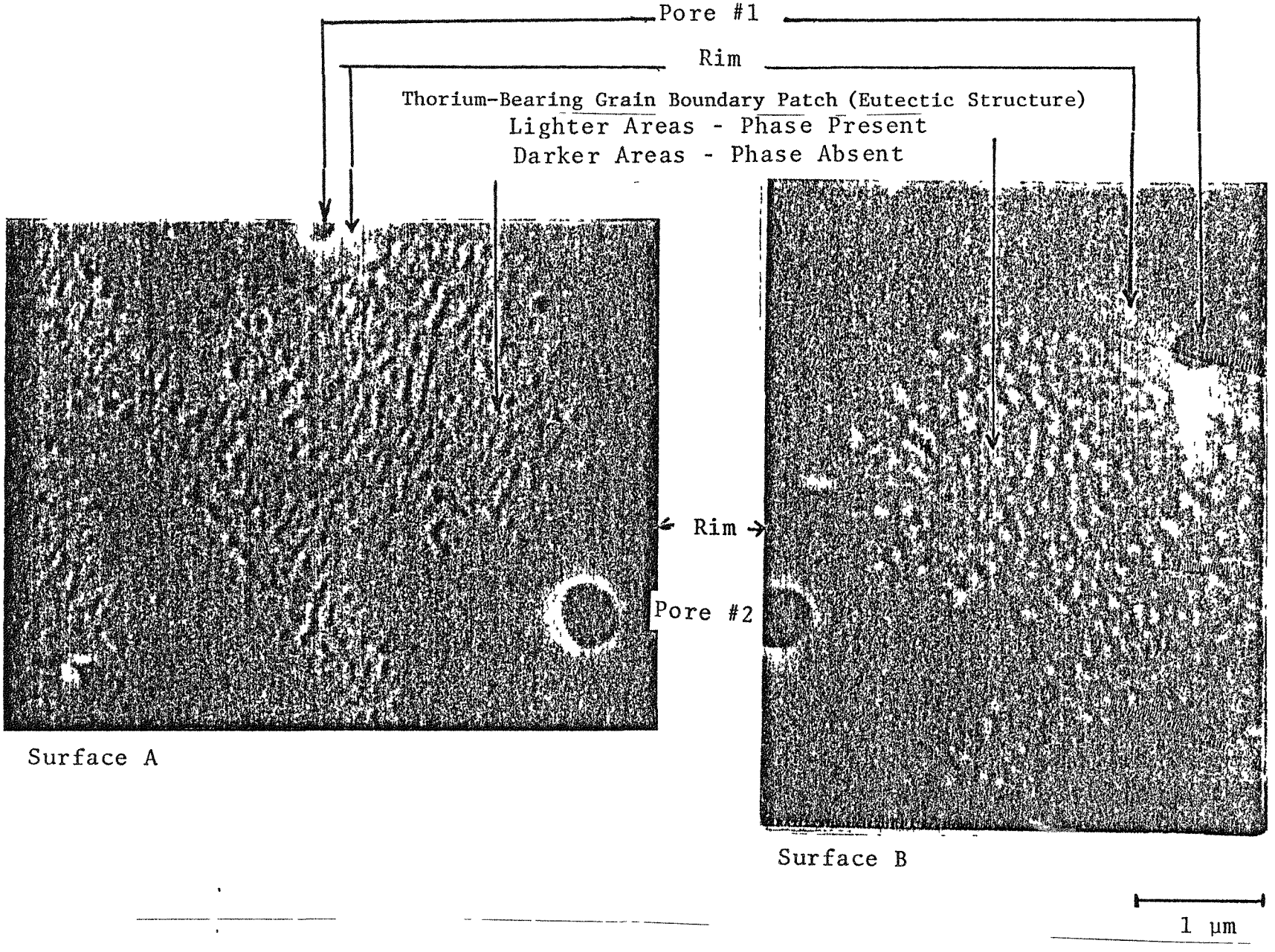


Figure 9. Structure of Distributed Submicron Pores on Mating Grain Boundary Surfaces in Welded Area of CVS T36

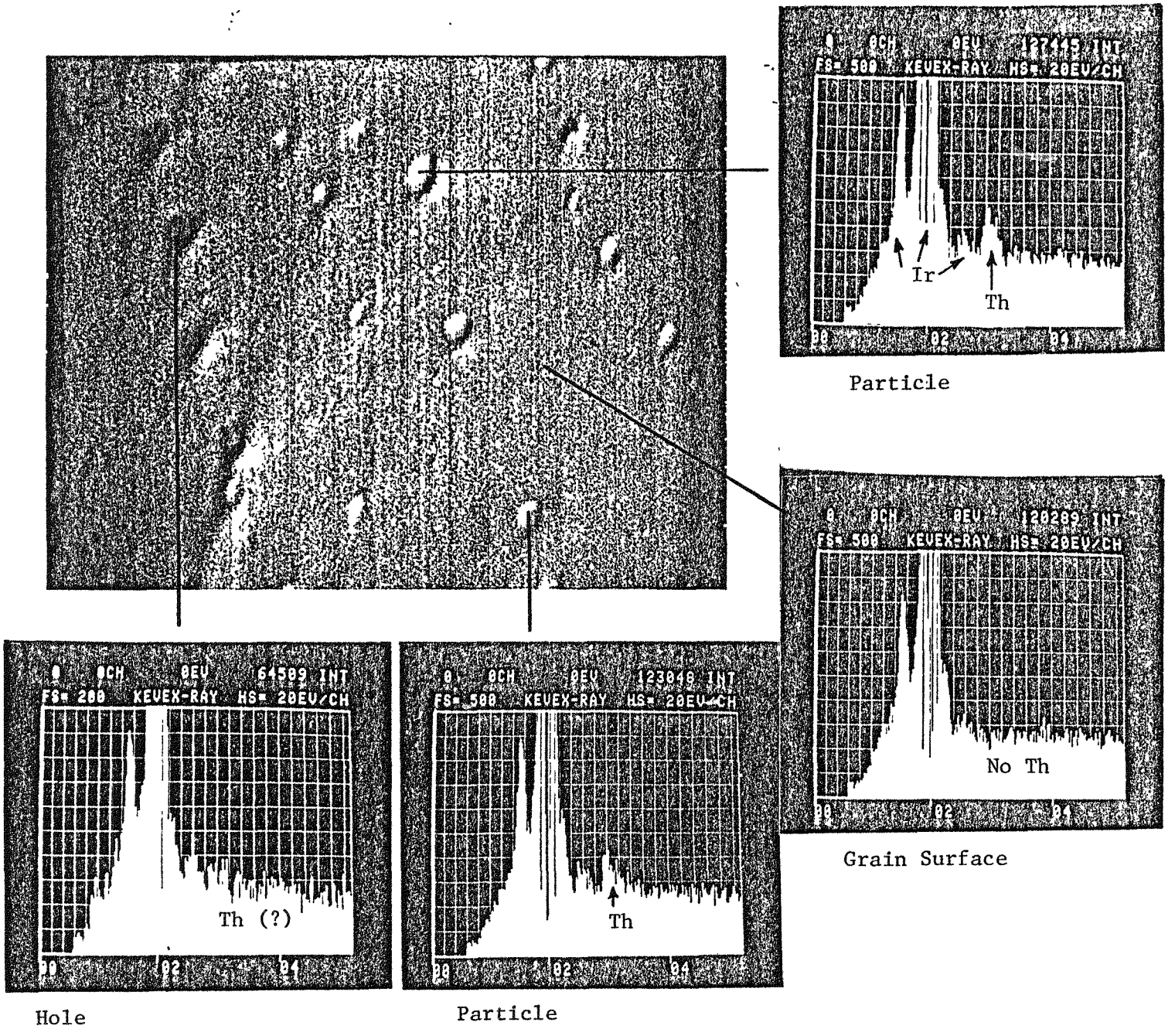


Figure 10. SEM/XES Analysis of a Grain Surface in Welded DOP-26 Alloy in CVS T24 Showing Thorium-Bearing Particles

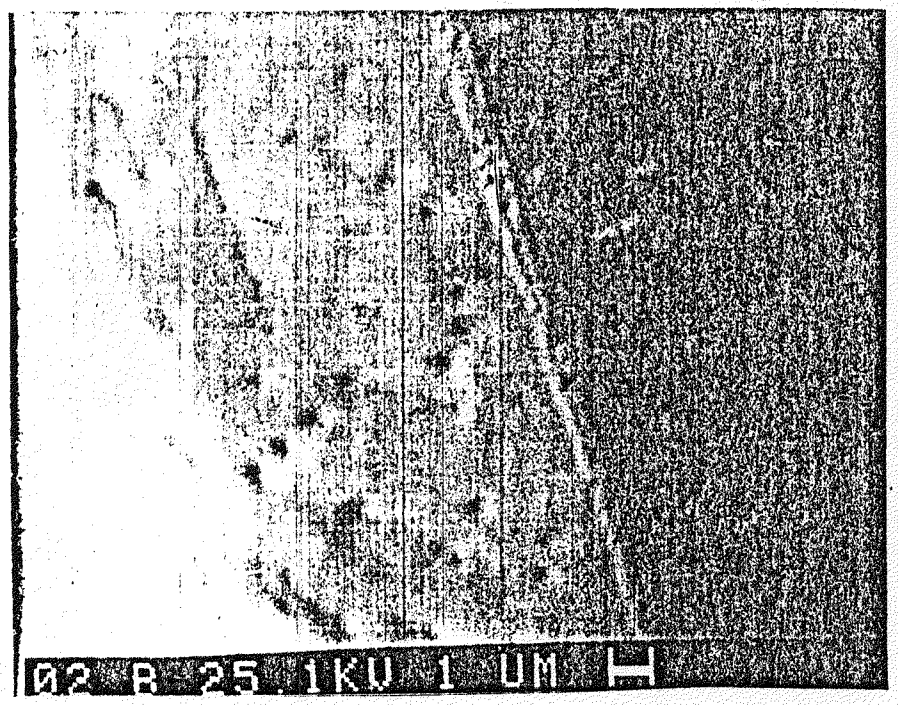


Electron Image

CVS T2

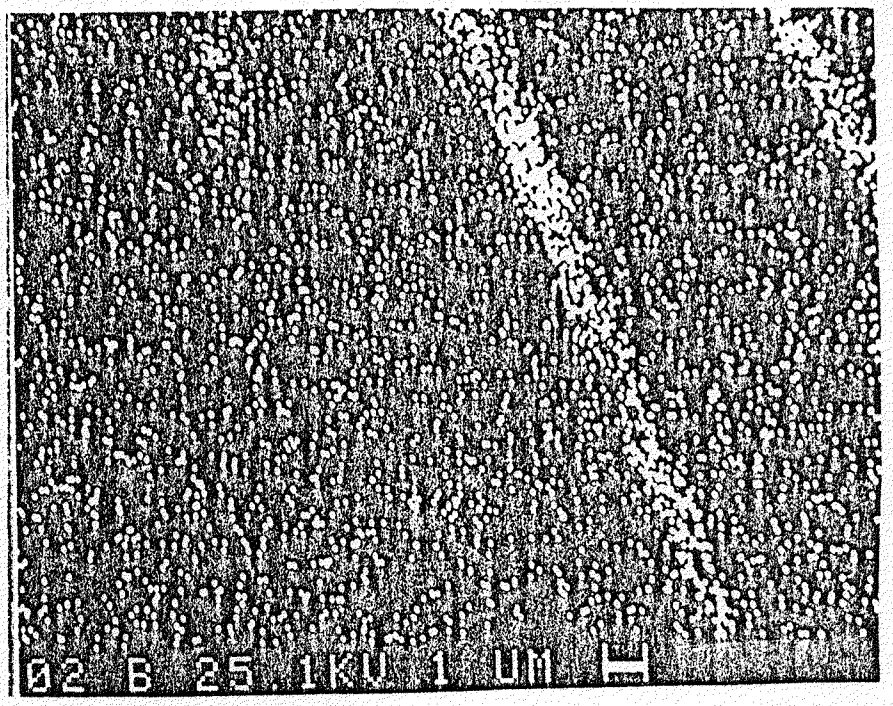


Thorium Map

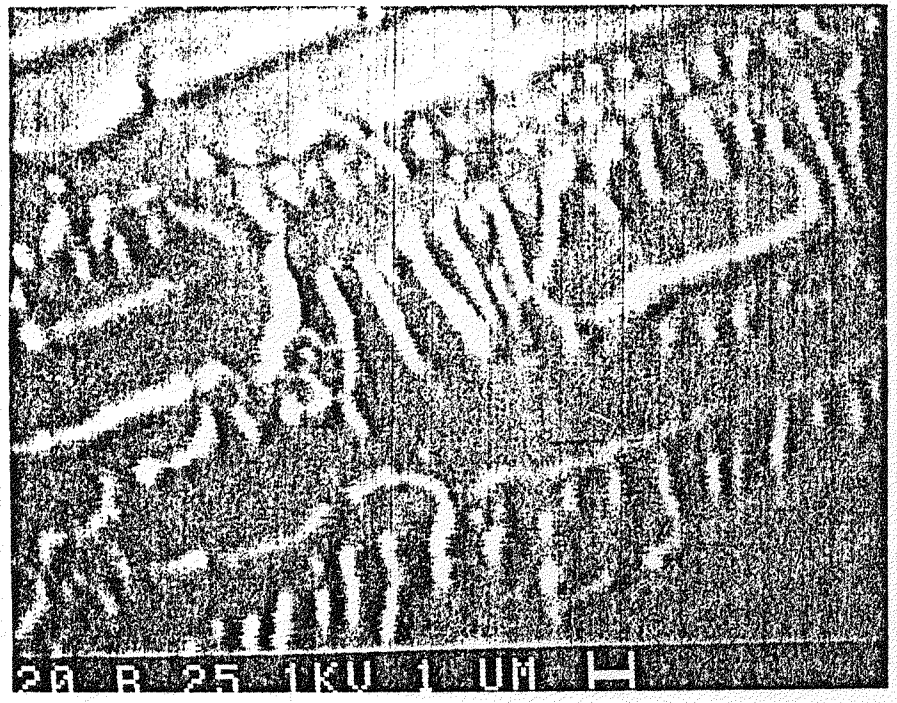


Electron Image

CVS T20


Thorium Map

Figure 11. EMPA of Grain Surfaces in Welded DOP-26 Alloy Showing Thorium-Bearing Stringers

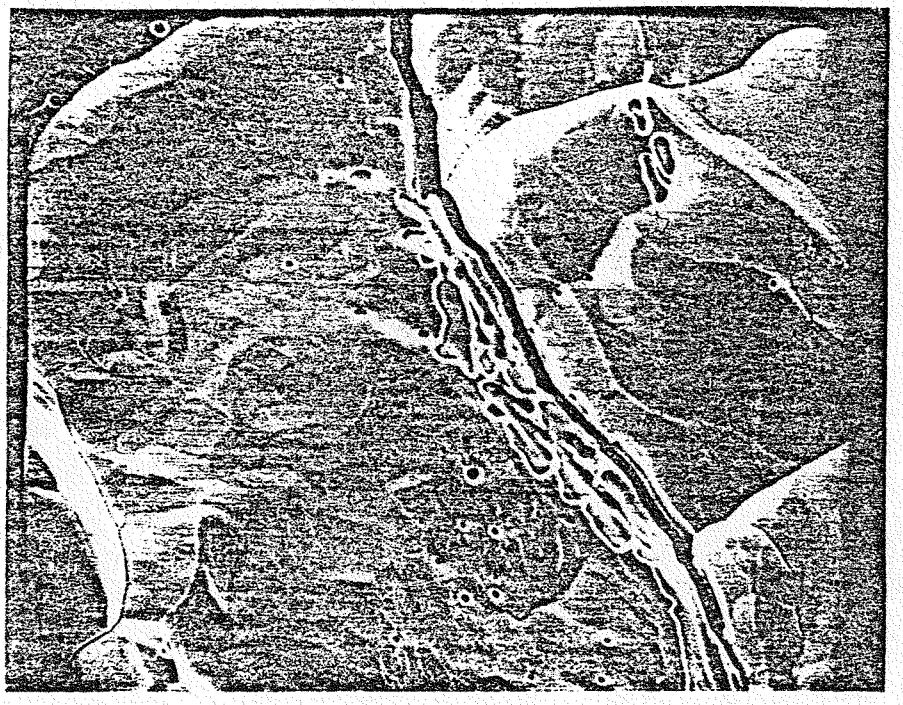


Figure 12. Pores and Grain-Edge Depressions in the Heat-Affected Zone of the Weld Quench Area on CVS T36

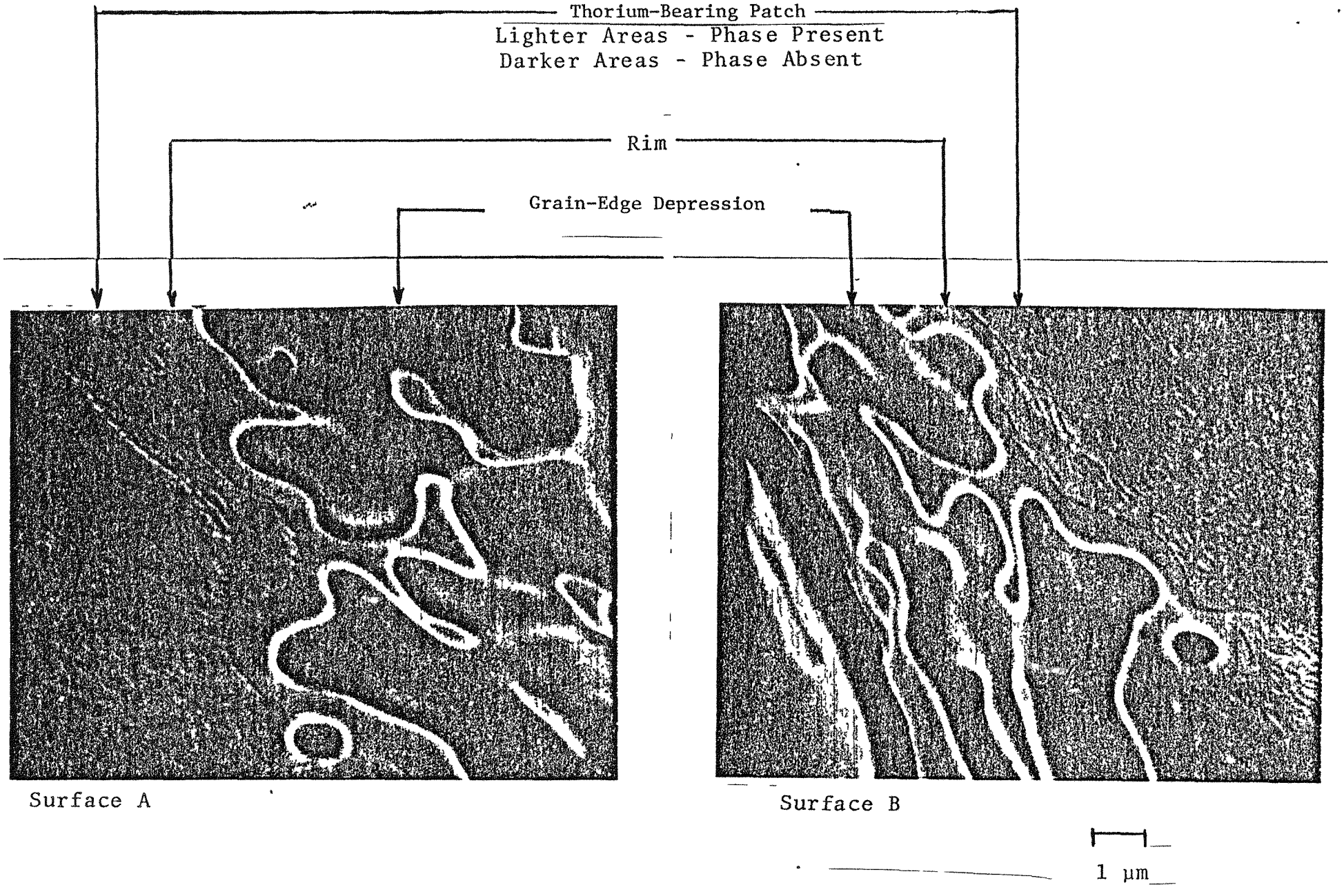


Figure 13. Structure of Grain-Edge Depression on Mating Grain Boundary Surfaces in Welded Area of CVS T36

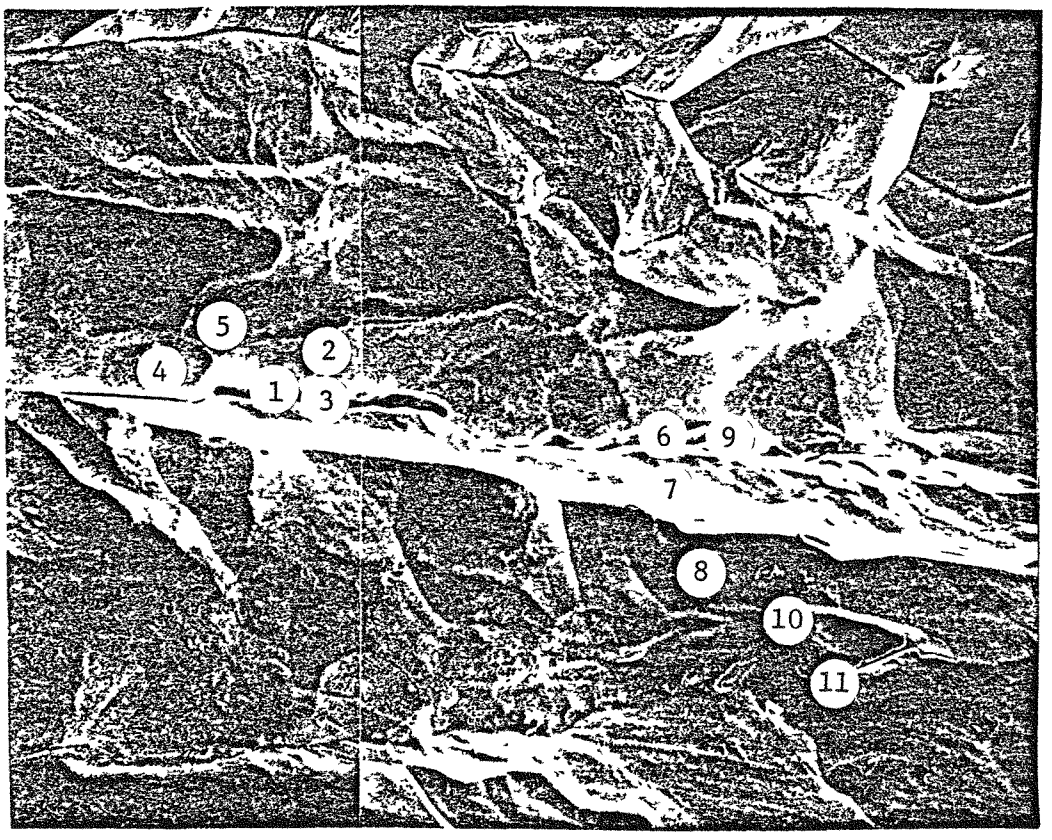


Figure 14. Points near Grain-Edge Depression on Grain Surfaces in the Heat-Affected Zone of the Weld Quench Area on CVS T36 Analyzed with the SUPER SAM (See Table 7)

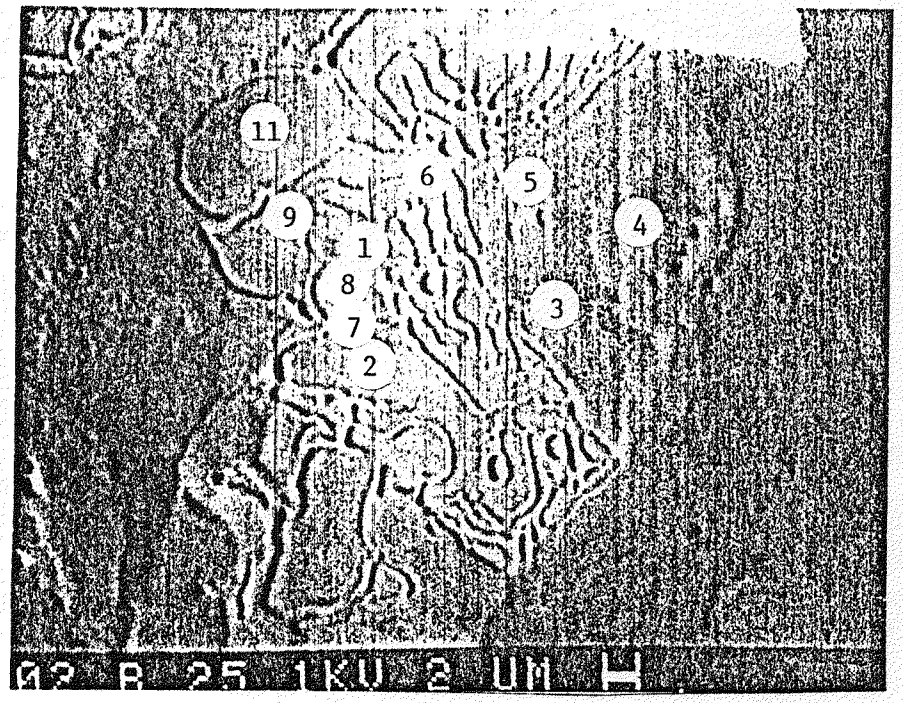


Electron Image

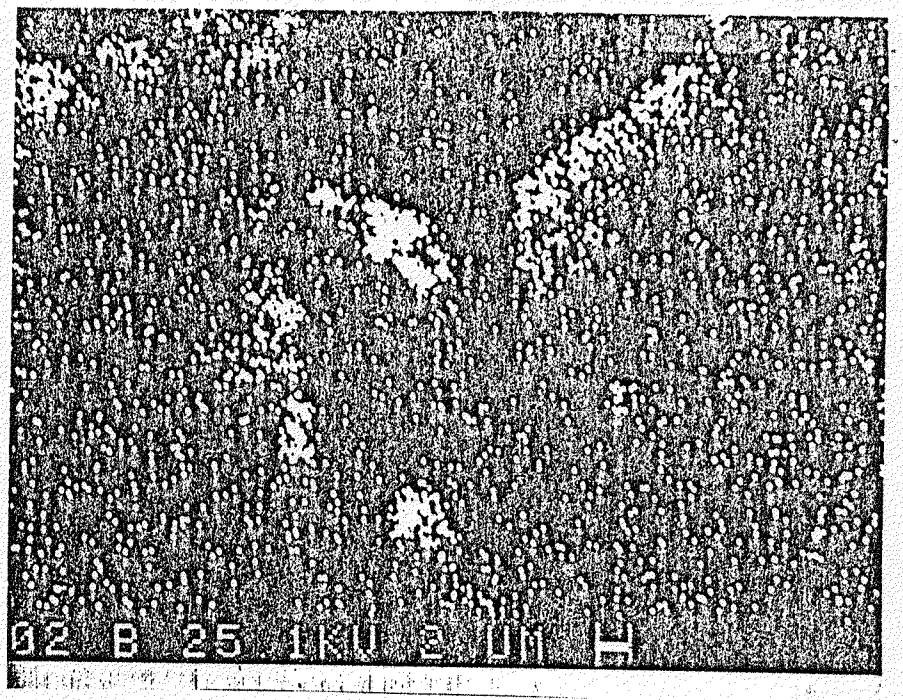


Th Map

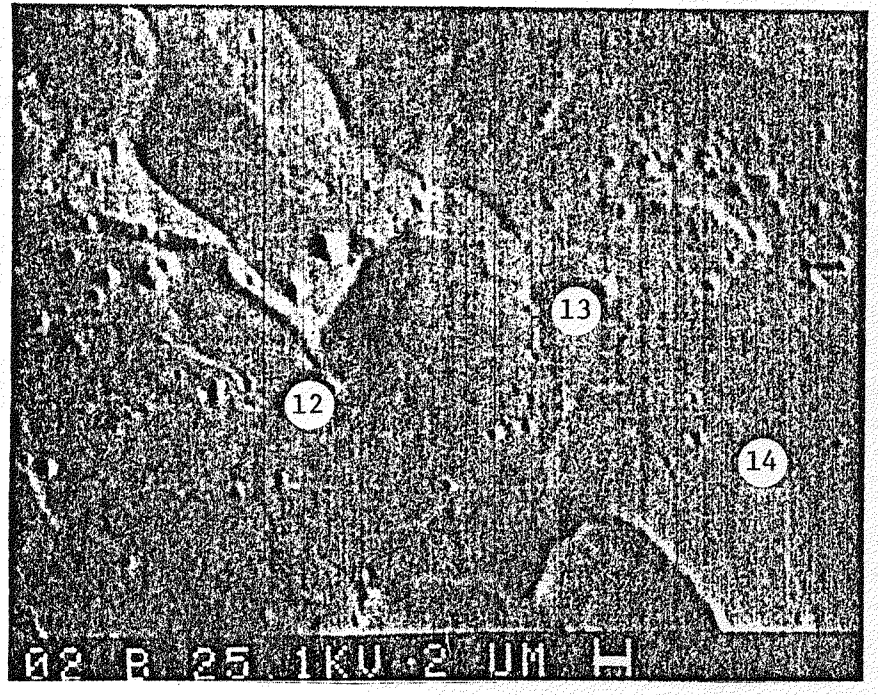


Electron Image

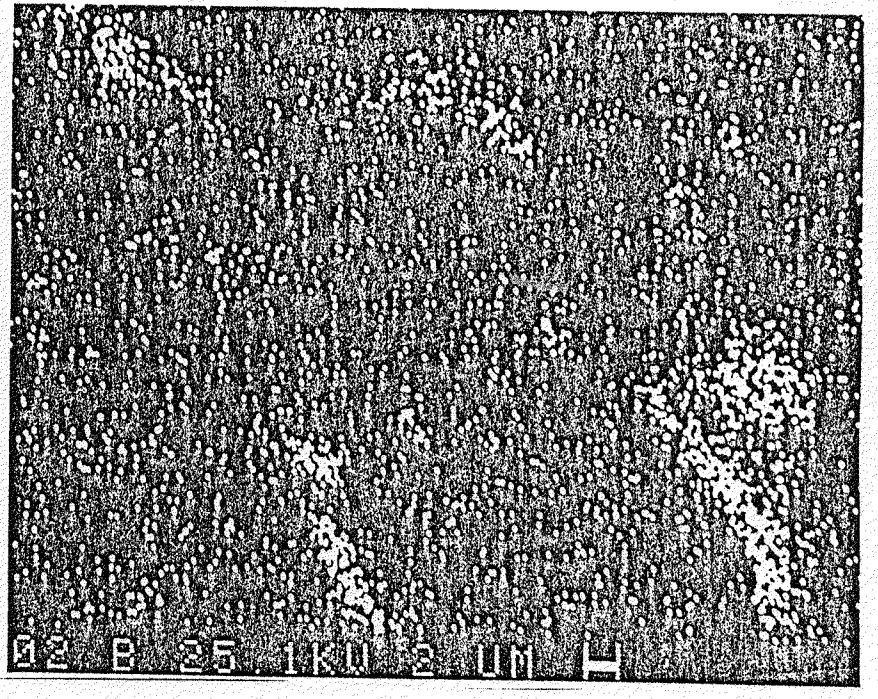


Th Map

Figure 15. EMPA of a Ridge Network in the Heat-Affected Zone of the Weld Quench Area on CVS T2 (See Table 8)

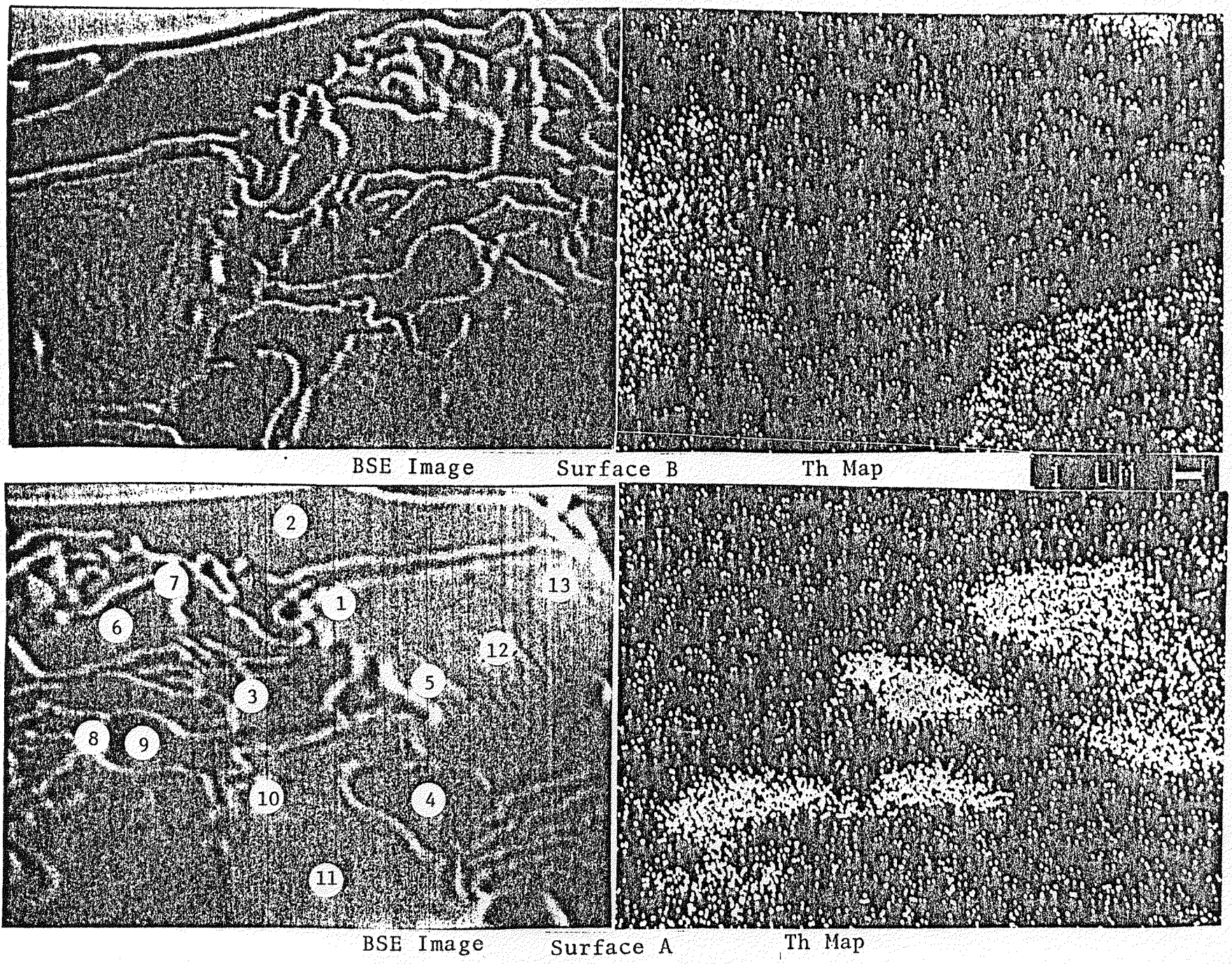


Figure 16. EMPA of a Ridge Network on Mating Grain Boundaries in the Heat-Affected Zone of the Weld Quench Area on CVS T2 (See Table 9)

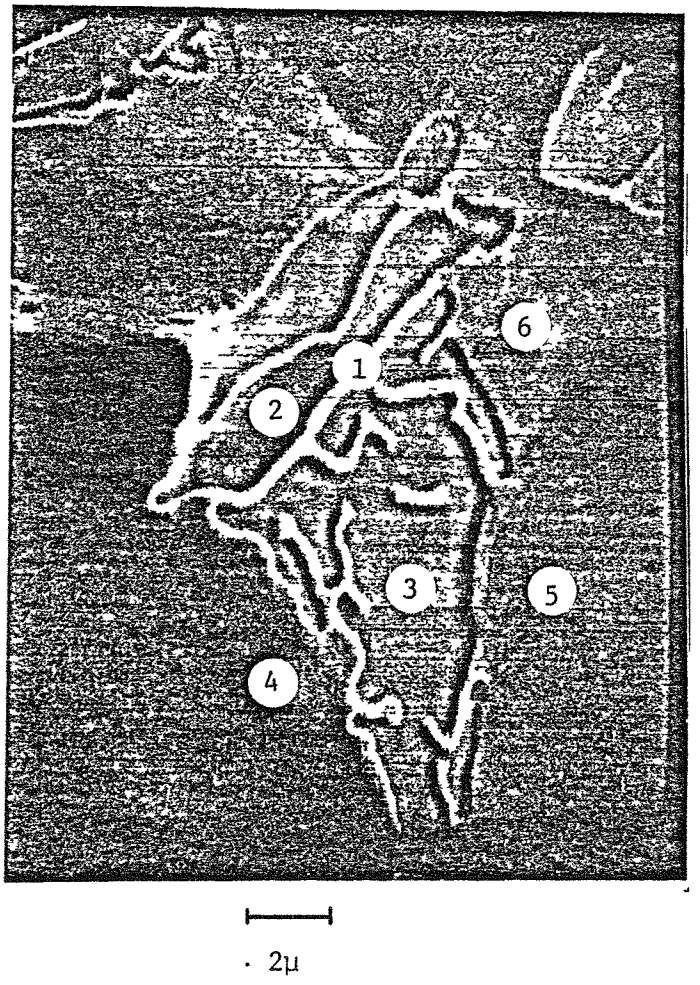


Figure 17. A Small Ridge Network in the Heat-Affected Zone of the Weld Quench Area on CVS T2 Analyzed with the SUPER SAM (See Table 10)

a. Fresh Fracture Surface

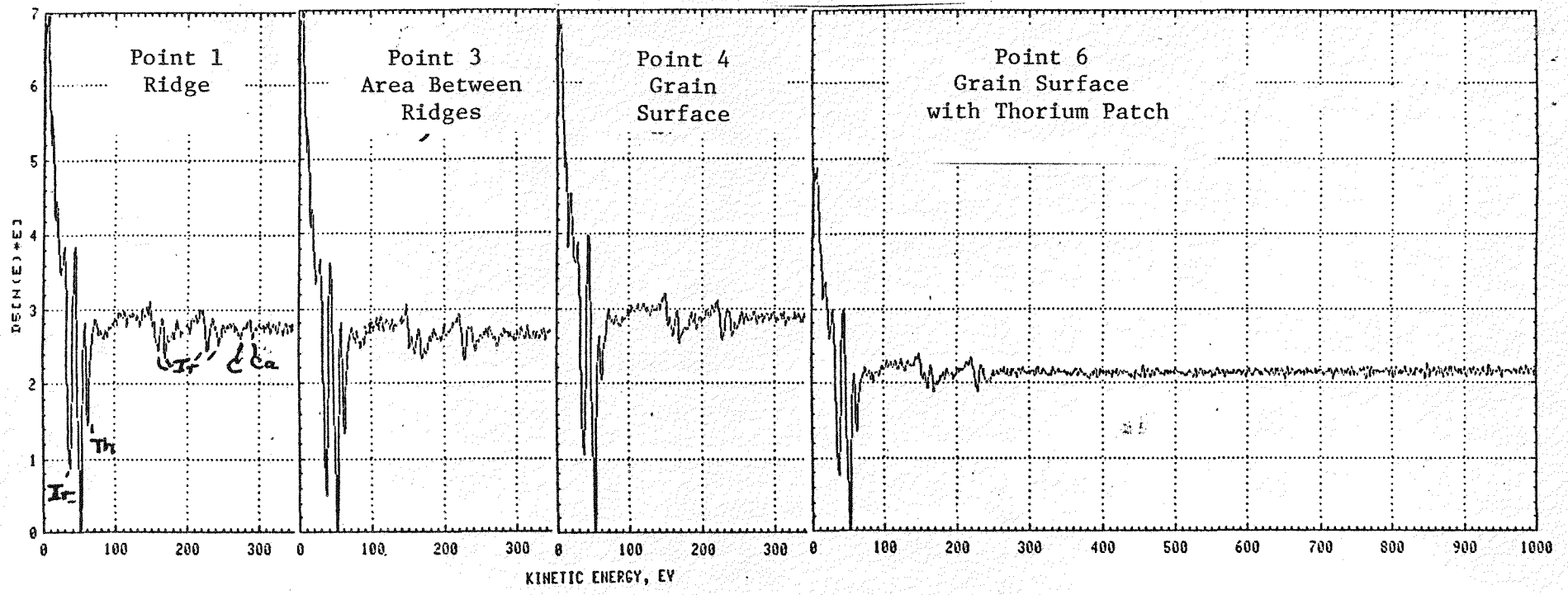


b. After 5-Minute Sputtering

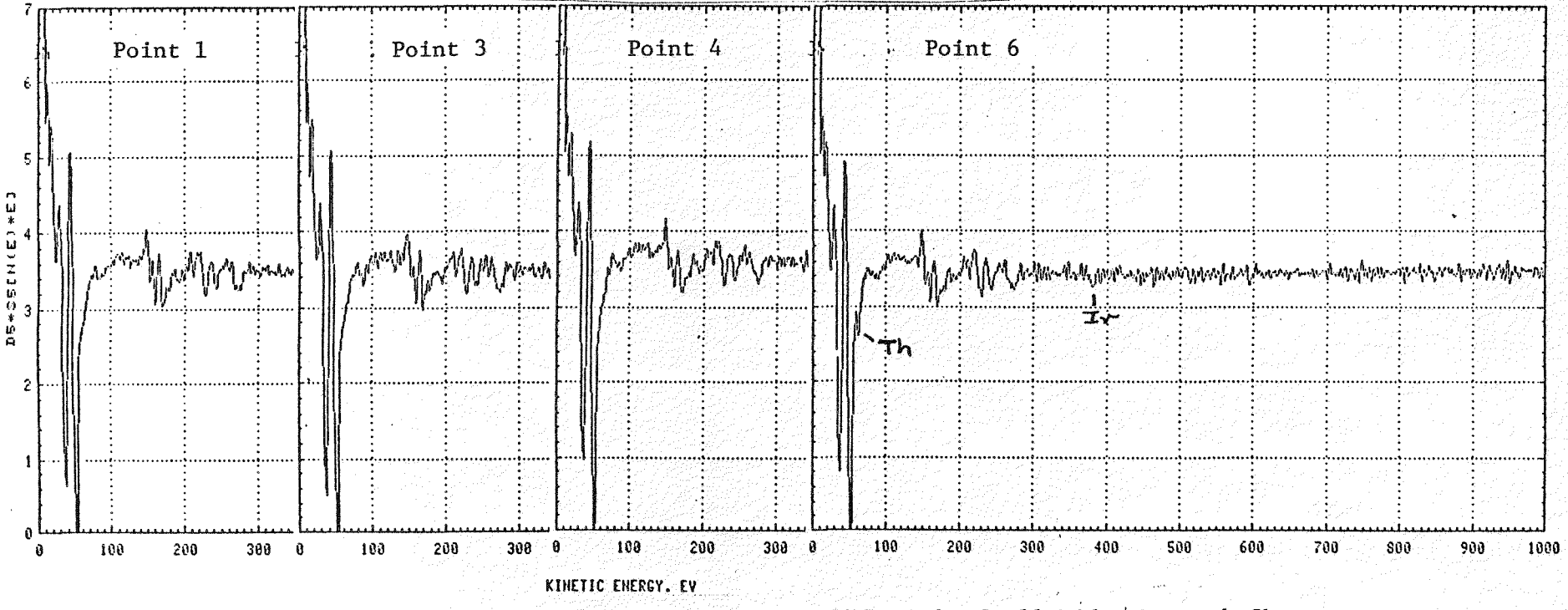


Figure 18. AES Spectra Recorded with the SUPER SAM on the Small Ridge Network Shown in Figure 17 (See Table10)

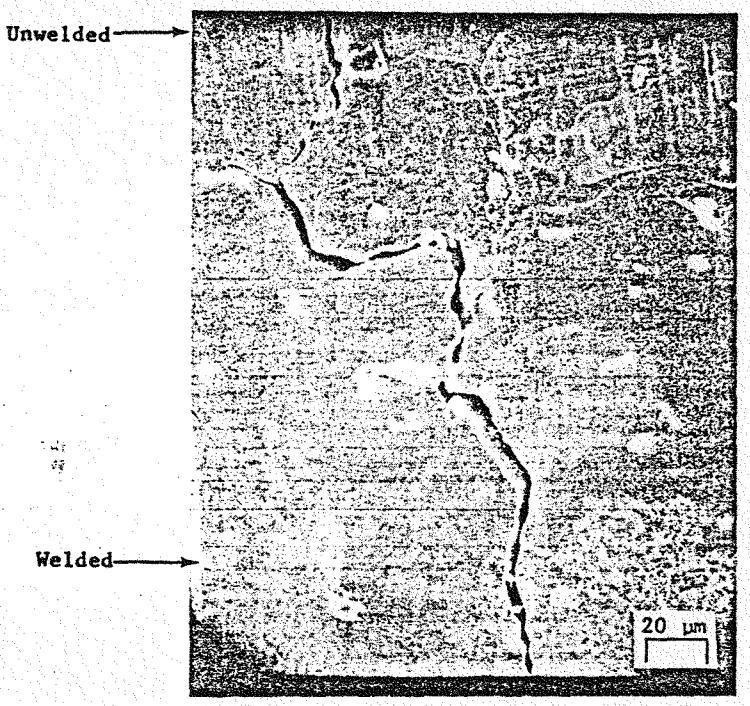


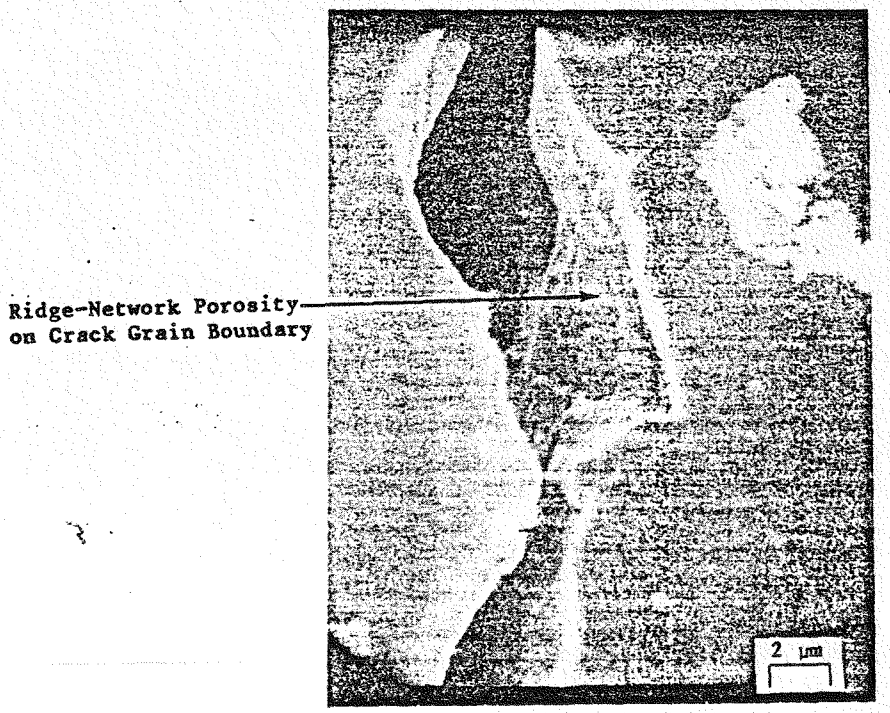


Figure 19. A Weld Quench Crack in CVS T36.

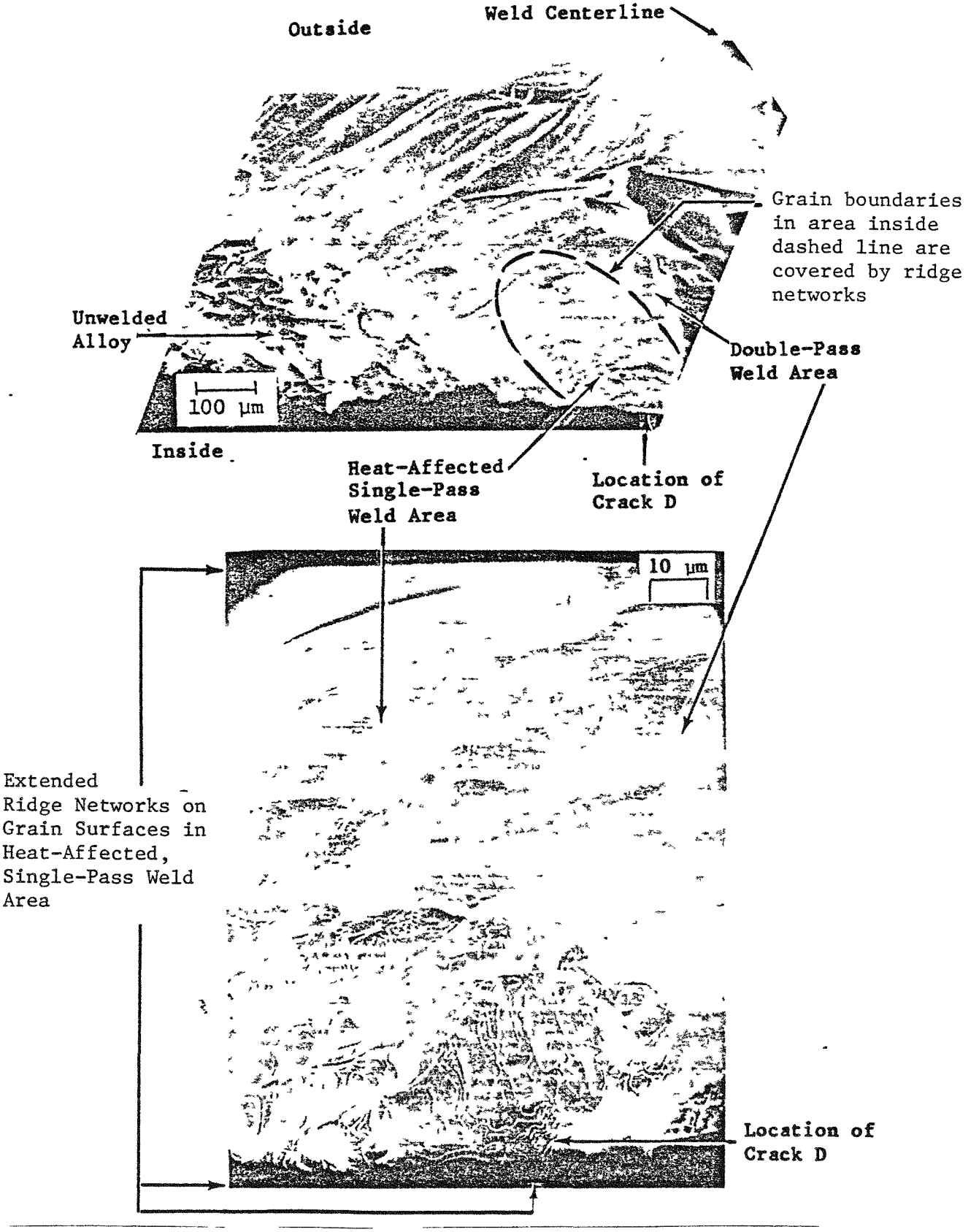


Figure 20. Grain Surfaces Exposed by Fracturing the CVS T36 Specimen Along the Weld Quench Crack Shown in Figure 19.

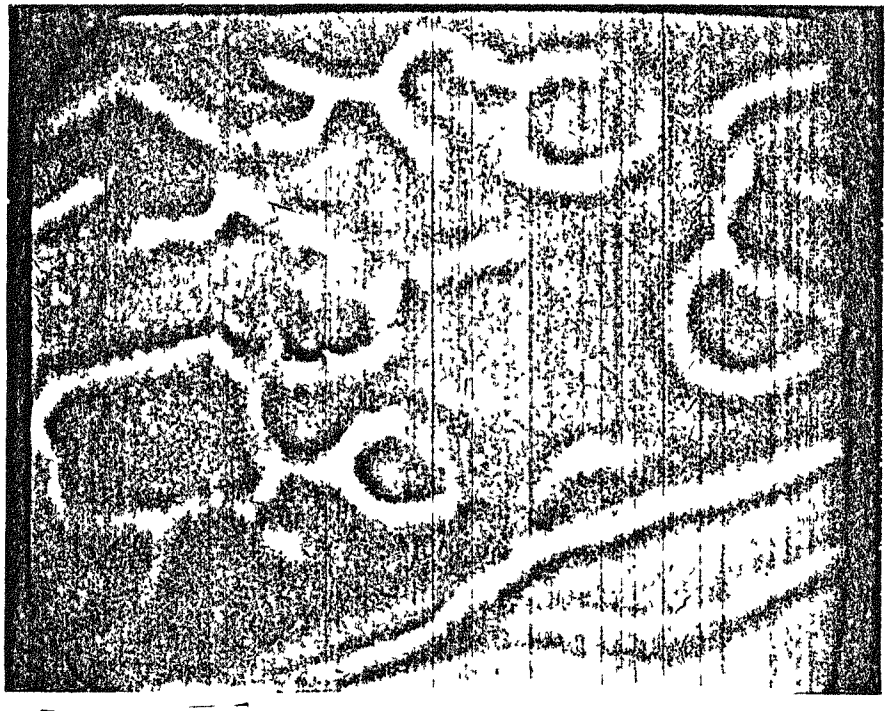

Surface A

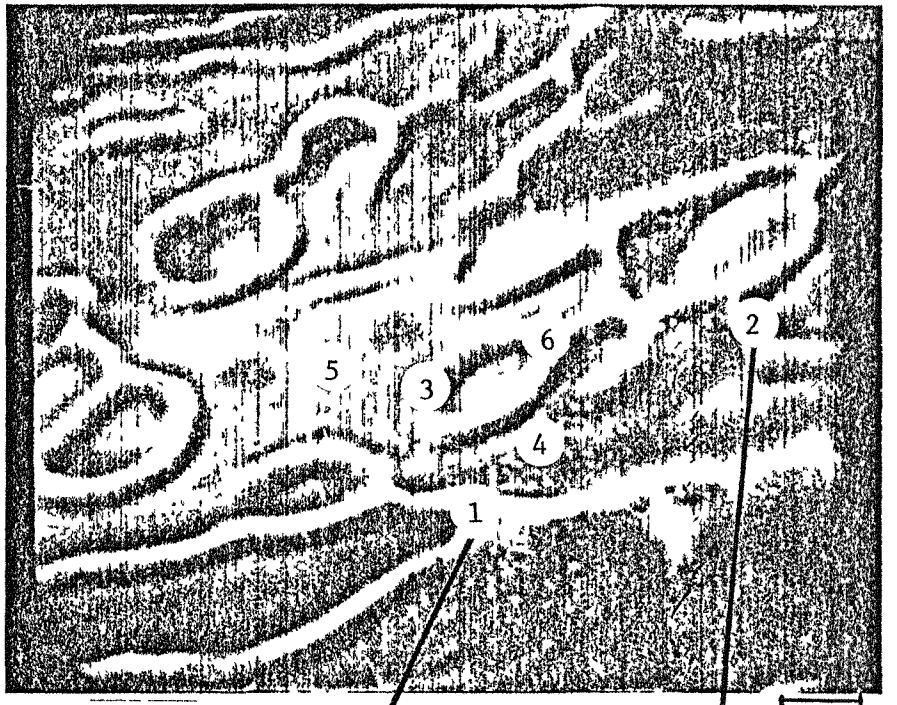


Surface B

1 μm

| POINT | RESULTS |
|---|---|
| 1 | Thorium detected by XES |
| 2 | Thorium detected by XES |
| 3 | No thorium detected by XES |
| 4 | 0.95 wt. % thorium detected by EMPA |
| 5 | 0.09 wt. % thorium indicated by EMPA |
| 6 | No thorium detected by XES |

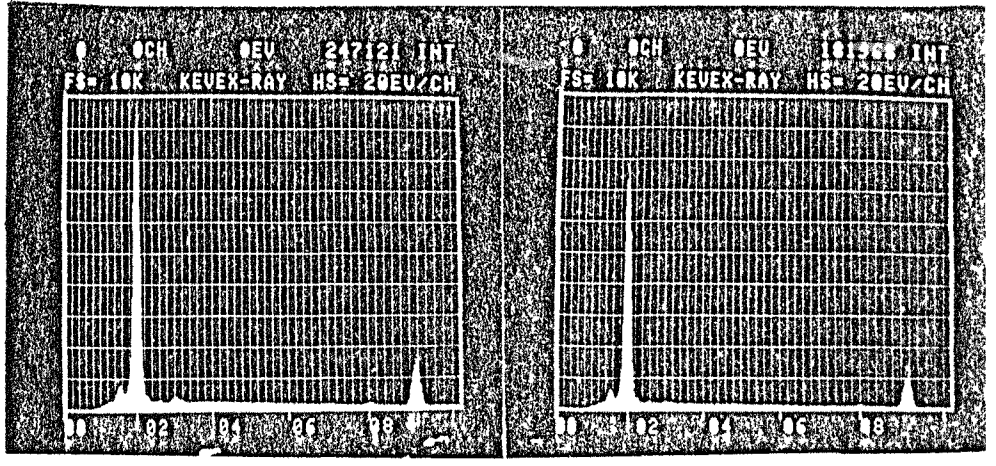


Thorium $M_\alpha$ peak at 3.0 KeV.
All other peaks from Iridium.

Figure 21. Structure of Ridge Networks on Mating Grain Boundary Surfaces Along Weld Quench Crack in CVS T36. Small White Spots are Thorium-Bearing Particles

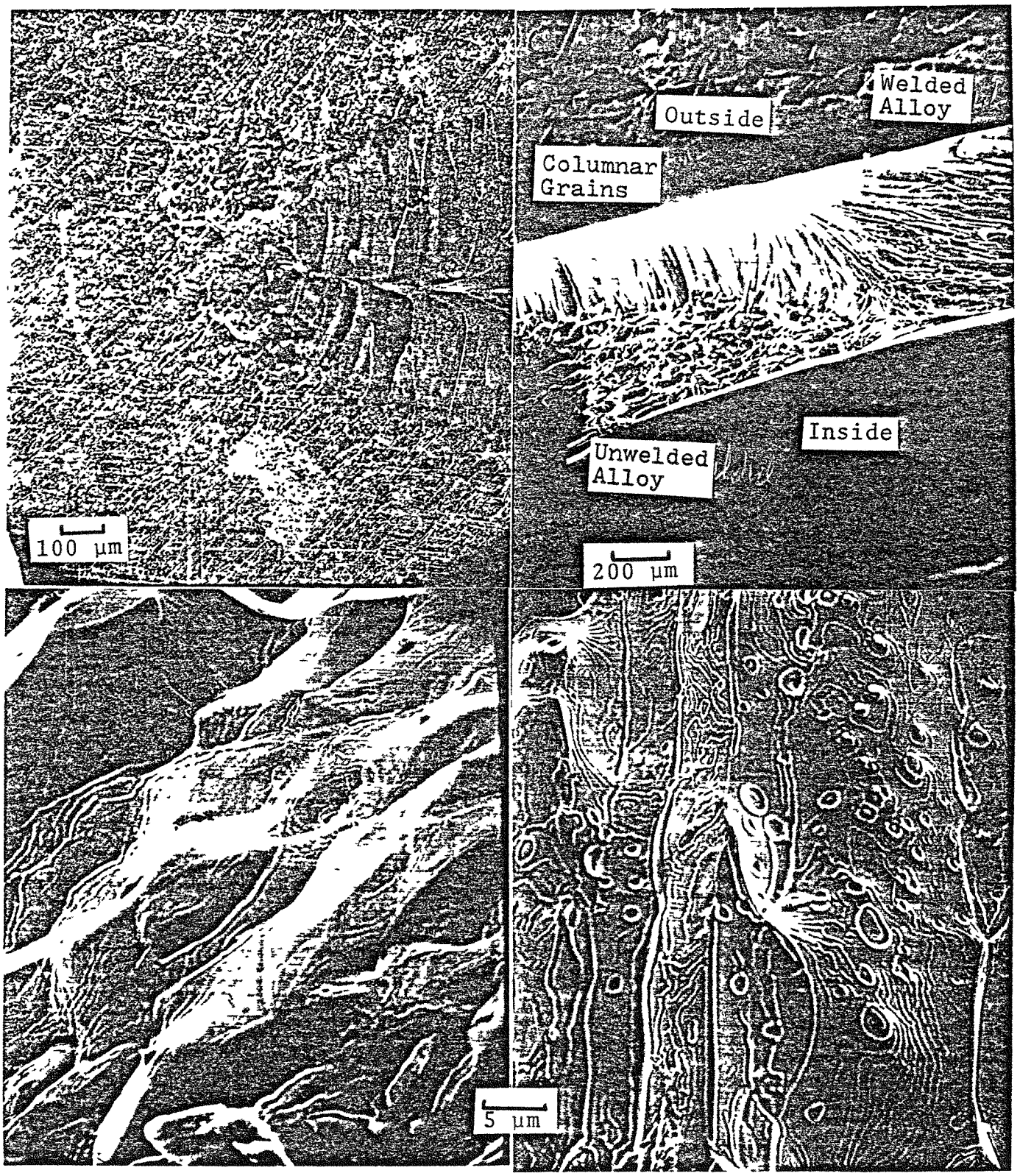


Figure 22. SEM Analysis of Weld Quench Area in Unwelded Alloy in CVS T39. (a) Cracks near tip of weld (b) Specimen fractured along weld centerline (c) Extended ridge networks on unwelded alloy grains in heat-affected zone (d) Extended ridge networks on columnar grains

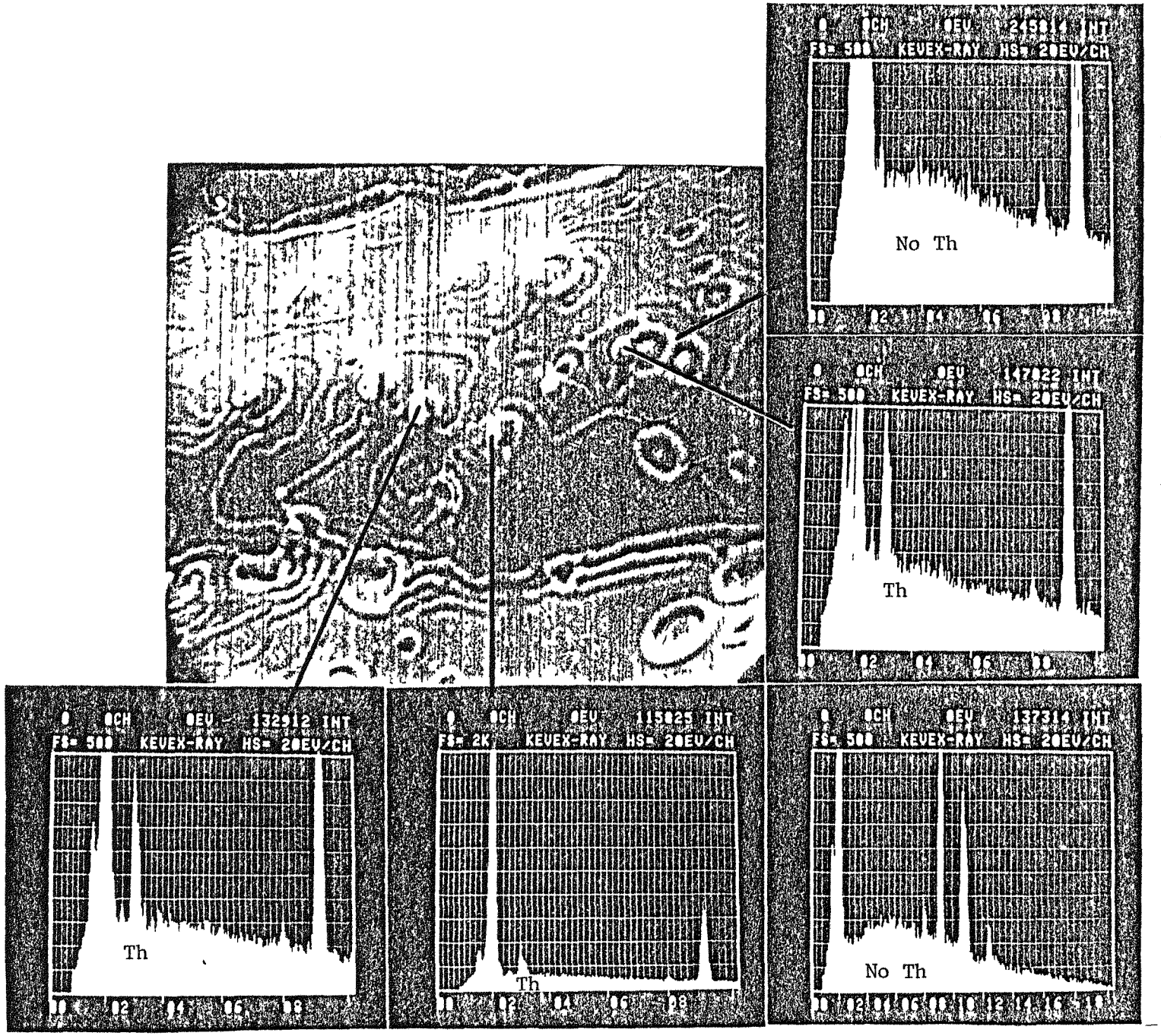


Figure 23. SEM/XES of Extended Ridge Networks on Columnar Grains in Weld Quench Area on CVS T39

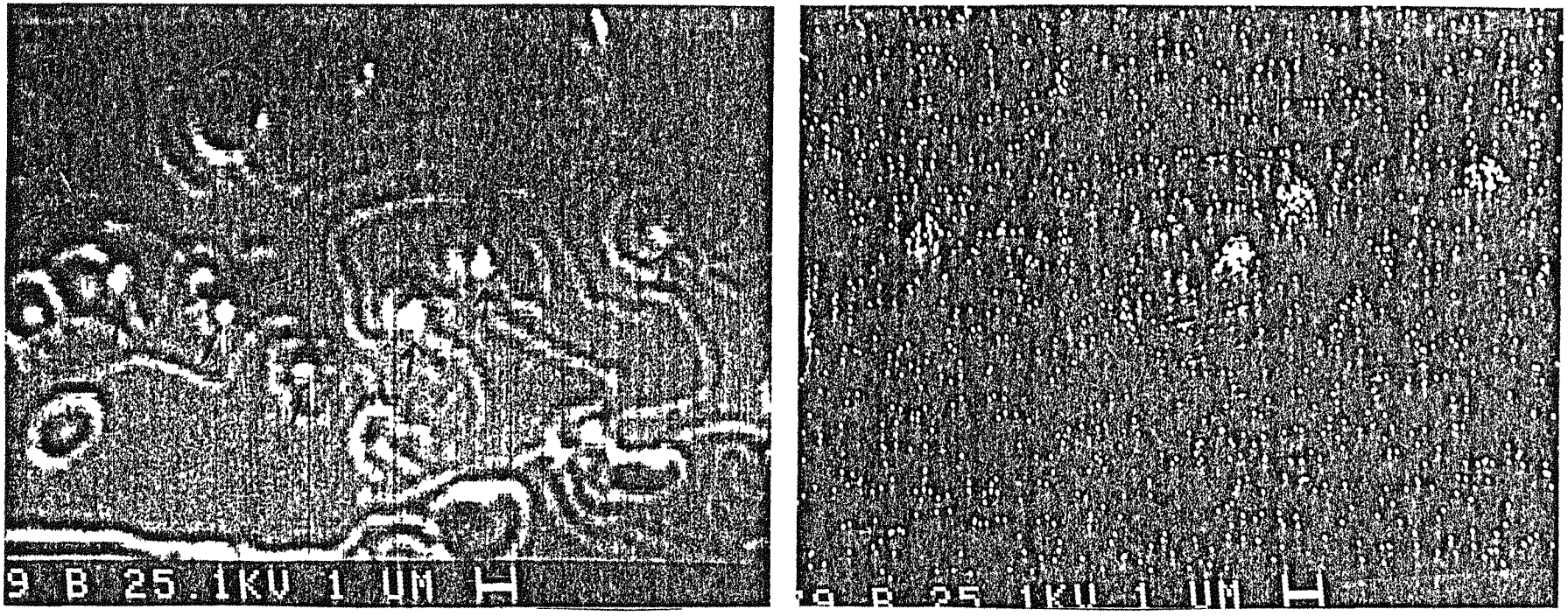


Electron Image

Thorium Map

Figure 24. EMPA of Extended Ridge Networks on Columnar Grains in the Weld Quench Area of CVS T39 Showing Thorium-Bearing Particles (Arrows)